UNIVERSITÀ DEGLI STUDI DI PADOVA

Dipartimento di Fisica e Astronomia "Galileo Galilei"

Corso di Laurea in Fisica

Tesi di Laurea

Study of low lying levels of ^{72}Ni

Relatori

Dr. Martha Liliana Cortés

Dr. José Javier Valiente Dobon

Laureando

Filippo Angelini

Anno Accademico 2019/2020

Contents

1 Theory Introduction **1**
1.1 The Nuclear Shell Model . . . 1
1.2 The Nickel Isotopic Chain . . . 2

2 Description of the experiment **3**
2.1 Experimental Apparatus . . . 3
2.2 Data Selection and Corrections . . . 4

3 Data Analysis **5**
3.1 `Geant4` Simulations . . . 5
3.2 Fitting procedure . . . 6
3.3 Fitted spectra and results . . . 7
3.3.1 Reactions spectra . . . 7
3.3.2 Coincidences spectra . . . 10
3.4 Experimental Level Scheme . . . 17

4 Results Discussion **22**
4.1 Shell Model Calculations . . . 22
4.2 Comparisons and discussions . . . 23

5 Conclusions and Perspectives **25**
5.1 Conclusions . . . 25
5.2 Future Perspectives . . . 25

Chapter 1

Theory Introduction

1.1 The Nuclear Shell Model

One of the most important models for the study of the nuclear structure was constructed from the observation of certain numbers (2, 8, 20, 28, 50, 82, 126) of nucleons, called **magic numbers**, which resulted in a particular stability of nuclei. Therefore, in analogy to the atomic energy shell structure, the idea of the **nuclear shell model** was born. This consists in the arrangement of the nucleons (in a separate way for protons and neutrons) into discrete energy levels which come from the solution of Schrödinger's equation for a single particle, interacting with a mean-field generated by the rest of nucleus, seen as a *core* of $A-1$ particles.

The initial model, using the harmonic potential as mean field, could only explain the first magic numbers, so the problem was better approached with a potential following the nuclear density profile, called Woods-Saxon potential. In addition to this, a key correction to the levels was found in the **Spin-Orbit interaction** (SO). The effect of this energy term was to take into account the alignment of the spin of the nucleons with the orbital angular momentum, resulting in a splitting of the energy levels depending on the nucleons total angular momentum and a redefinition of the energy gaps between levels. With SO corrections, the scheme of the nuclear shells was complete and the magic numbers, corresponding to relatively large gaps between energy levels (see Fig. 1), were predicted correctly by the theoretical model [1–3].
Further investigations in the latest decades, though, revealed that in the most exotic regions of the chart of nuclides, new magic numbers arise and some disappear and this behaviour has been called **shell evolution** [4].

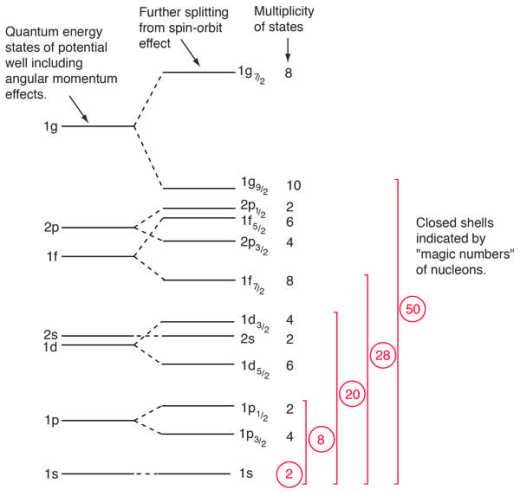

Fig. 1. Energy levels of the nuclear shell model and magic numbers [5]

This change in the gaps between energy levels has its explanation in the fact that the nucleon-nucleon interaction [4] is not fully characterised in the mean-field potential approximation of the shell model. There have been different ways to explain the modifications in the energy gaps: firstly, the mean-field potential and the energy of the single-particle levels are modified dependently on the radial distribution, angular momentum and spin of nucleons in different orbits. In second place there could be a weakening of the spherical shell gaps, caused by correlation of pairing or quadrupole type, that could deform the nucleus and cause changes in the single-particle levels. Lastly, interactions between bound states, resonances and scattering states could act on the properties of weakly bound nuclei [4]. At different degrees of approximation, theoretical calculations can be made to understand better the evolution of the energy gaps from the interaction between nucleons. A powerful method is to model an inert core nucleus, starting from experimentally measured energy values, and study the **effective** two-body interactions of the most external nucleons, confined in what is called valence space. The most recent shell model calculations start from a determined double-magic nucleus and numerically compute the energy levels through the effective interaction, which takes into account both the nucleon-nucleon force and the effect of the core-generated mean field [4]. To quantify the intensity of the nucleon-nucleon interactions, the main coefficients are the **Two-Body Matrix Elements** (TBME). These depend on the shells occupied by the two particles and especially on their angular momentum. From these matrix elements a function is constructed, which averages the TMBE, weighing them on the degeneracies of the total angular momentum $\vec{J}$, and represents the effective interactions between

nucleons. This is called **monopole term** and its changes lead to the evolution of the spherical shell structure. Furthermore, in the mean-field approach, the SO interaction is proportional to the radial derivative of the nuclear density, therefore it is peaked around the surface of the nucleus. Hence it is argued that in neutron-rich nuclei with a higher surface diffuseness, i.e. a less packed distribution of neutrons around the surface, a reduction of the SO term determines smaller shell energy gaps [4]. Apart from this mean field observation, it was proposed that the tensor interaction between proton and neutron, an additional term in the nucleon-nucleon interaction, could change the energy splitting when specific orbits are filled [4, 6]. The main focus of the present work is to investigate the properties of the ^{72}Ni isotope, therefore it is required a more detailed introduction for its shell model configuration.

1.2 The Nickel Isotopic Chain

Nickel corresponds to $Z = 28$, which is a magic number that originates from the spin-orbit coupling. The shell closure at 28 comes from the lowering of the $1f_{7/2}$ sub-shell in the middle of the gap between the sd and pf oscillator shell due to the spin-orbit correction; this effect that can be observed also in Fig. 1. Therefore, the significant proton energy gap for the nickel is the one between $\pi f_{7/2}$ and $\pi p_{3/2}$ levels.

The isotopic chain of nickel is especially interesting because it covers a wide range of nuclei, meeting 3 neutron shell closures ($N = 20, 28, 50$) and a harmonic oscillator shell gap ($N = 40$), therefore it allows for the testing of the nuclear interactions in many different ways. The filling of the neutron orbits, from the $\nu f_{7/2}$ in the proton-rich isotopes up to the $\nu g_{9/2}$ for the neutron-rich, can cause specific proton-neutron interactions and result in effects of energy gap modifications for the evolution of the magic numbers. To study these effects, experiments have been conducted on the binding energies of the proton orbits, on energy of the first excited state $E(2^+)$ and reduced transition probability $B(E2; 2^+ \rightarrow 0^+)$ along this isotopic chain. Furthermore, a recent study of low-lying levels in ^{72}Ni was performed, which suggests that this isotope could be a significant point for shape coexistence in the nickel chain [7].

The nickel isotopes between the closures for $N = 28$ and $N = 50$ have been studied in many works. The experiments for the even-even isotopes show that the $B(E2; 2^+ \rightarrow 0^+)$ has local minima corresponding to the sub-shell closures with $N = 28$ and $N = 40$. In the region in-between, the measurements follow an inverted parabolic trend with a peak at around $N = 34$. The $E(2^+)$ values, instead, have a quite opposite behaviour: the highest values are reached in correspondence of the aforementioned closures, while, in the middle, the excitation energy floats around a lower constant value [4, 8, 9].

For the interval $N = 40-50$ it is predicted a similar behaviour to the region $N = 28-40$, that consists in an inverted parabolic trend for the $B(E2)$ and a rather constant $E(2^+)$ peaked at the two closures. While the values of $E(2^+)$ are indeed constant [8] and its recent measurement in ^{78}Ni confirms the conservation of the $Z = 28$ and $N = 50$ magic numbers far from stability [10], the behaviour of the $B(E2)$ is still not entirely clear, given that reported values do not follow a parabolic trend [9, 11, 12].

Another interesting aspect about the semi-magic structure of Nickel is the arising of seniority isomers in the even-even isotopes. The seniority ν is a quantum number that indicates the number of nucleons that are not paired with total angular momentum $J = 0$ [13]. In ^{70}Ni and ^{76}Ni, the yrast 8^+ state has been observed to have a lifetime in the range of μs, while in ^{72}Ni and ^{74}Ni, the former with 4 neutrons and the latter with 4 neutron-holes in the $\nu g_{9/2}$ subshell, this behaviour disappears. A hypothesis for this phenomenon is the lowering in energy of the 4^+ and 6^+ states with $\nu = 4$, that allows for a more probable decay from the 8^+ state, decreasing its lifetime [14, 15]. In ^{72}Ni, the lifetime of the 6^+ state with seniority $\nu = 4$ has been measured and its value is in the order of magnitude of ns [15], meaning that if a nuclear reaction were to populate this state, the long lifetime could have an effect on the spectroscopic analysis of the transitions between the energy levels below it.

The present works aims at studying the nuclear structure of ^{72}Ni through the comparison of the population of low-lying states from two different reaction channels: proton knockout from ^{73}Cu, and neutron knockout from ^{73}Ni [16]. A similar analysis was conducted on the neighbouring even-even isotope ^{70}Ni [17] with a focus on the proton-knockout reaction channel and the comparison with those result could highlight the similarities and the differences in the isotopes.

Chapter 2

Description of the experiment

2.1 Experimental Apparatus

The experiment was performed at the Radioactive Isotope Beam Factory, operated by the RIKEN Nishina Center and Center of Nuclear Study of the University of Tokyo during the first SEASTAR campaign [18]. Different beams of radioactive species were produced via the in-flight method, accelerating ^{238}U to an energy of 345 MeV/nucleon and striking it on a ^{9}Be target to produce neutron-rich isotopes through induced fission. The acceleration of the U beam was performed in multiple stages with the aid of four consecutive cyclotrons, in order to reach the fixed energy. The secondary beam, stripped of all its electrons, entered the two-stage separator called BigRIPS [19]. This consisted in a magnetic spectrometer [20] to separate the produced isotopes by the ratio of their number of mass over their charge, A/Q, and their atomic number Z. The device (as can be seen in Fig. 2) was composed of a series of magnetic dipoles for the separation among different A/Q ratios, superconducting quadrupole triplets for focusing the beam, and wedge-shaped degraders to achieve separation in atomic number. The separator is described as achromatic because it provided spatial separation of the isotopes regardless of their momentum. Several detectors were set up in BigRIPS: thin gas detectors were utilized for making position measurements across the focal plane, to relate the particle trajectories (their magnetic rigidity $B\rho$) to their A/Q; plastic scintillators were employed to have *time-of-flight* measurements over a known distance and to extract consequently the velocity of the particles; an ionization chamber was used to get a measure of energy loss from the flying nuclei, which is proportional to Z^2. Thanks to this separation process, at the end of BigRIPS, it was possible to fully identify the species of the incoming nuclei on an event-by-event basis. Once the secondary beam of the selected isotope exited the separator, it was focused on MINOS [21], the device used as target. This consisted of a 100 mm-thick cilynder of liquid hydrogen, surrounded by a concentric time projection chamber [22] that helped determine the reaction vertex. When the particles in the beam had a nuclear reaction with the protons (hydrogen) in the target, the heavy isotopes continued flying forward due to the high velocity. As a product of reactions, they could result in an excited state and emit consequently γ-rays to get to the ground state. For the daughter-nuclei in the reactions, an identification was performed with the ZeroDegree spectrometer [19]. The structure of this achromatic separator was similar to BigRIPS's (Fig. 2), as it was made of two magnetic dipoles and several quadrupoles, in order to separate and identify the isotopes coming from the target. At software level, the data from a single reaction got selected with coincidences of the wanted isotopes both before and after the target.

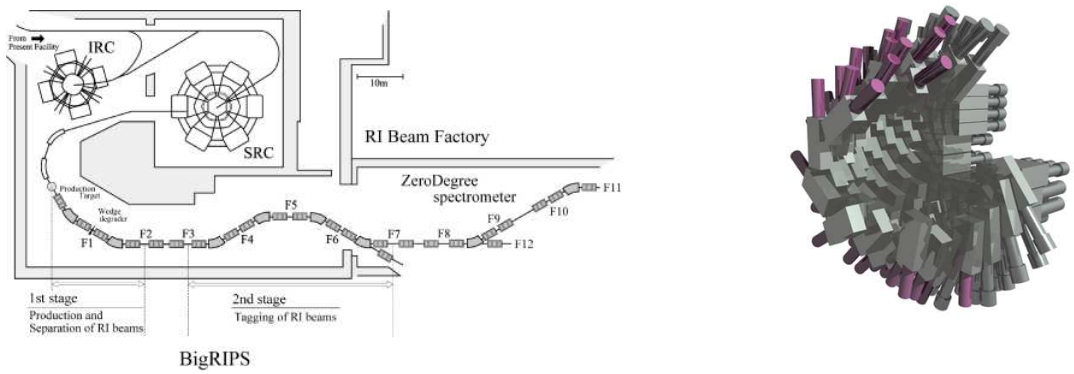

Fig. 2. Schemes of the experimental apparatus from Ref. [23]. The left image is a scheme of the two separators BigRips and ZeroDegree without the detection array. The right image is a 3D model of the section of DALI2.

The γ detection array, DALI2 [24], was positioned around the MINOS target to detect the γ-rays emitted by the fragments after the reaction. The array was made of 186 NaI scintillators, covering a large solid angle (Fig. 2). The light signals from the crystals were read out with photo-multiplier tubes and then fed into a shaping amplifier to get measurements of time and energy. The energy resolution of the array was estimated around 8% (FWHM) at 662 keV, while the time resolution was about 2 ns [24, 25]. The time window that identified an event had a duration of few μs.

2.2 Data Selection and Corrections

Once the data from all possible isotopes created from the fission of the primary beam was gathered, at a software level some elaboration was needed. The event-by-event identification allowed for a practical selection of the wanted isotopes by gating on the correct A/Q as well as Z. The selection was made for both the mother nucleus in BigRIPS and for the daughter nucleus in ZeroDegree (see Fig. 3). In the present work, the reactions taken into account are the ^{73}Cu$(p, 2p)^{72}$Ni proton knockout and the ^{73}Ni$(p, pn)^{72}$Ni neutron knockout. Since the analysis is based entirely on the study of the γ spectra from DALI2, some operations were needed before the final interpretation. In particular, a Doppler correction and an Add-back procedure.

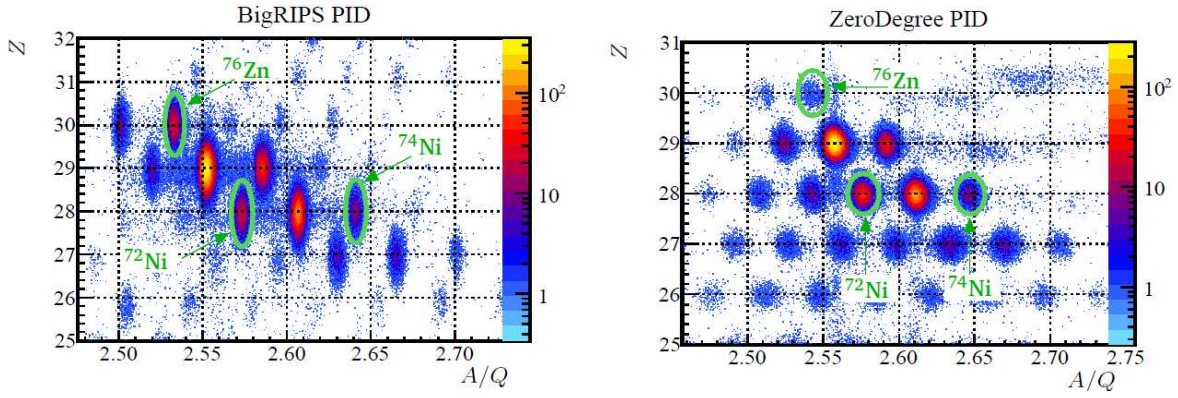

Fig. 3. Particle Identification (PID) in BigRips (left) and in ZeroDegree (right). The plots show the distribution of counts depending on atomic number Z and ratio A/Q. The green circles represent the gates for isolating the single isotopes in the data. Figure taken from Ref. [25].

The excited daughter nuclei that emit γ-rays after the reactions are travelling at a relativistic speed βc. Therefore, a photon emitted at a certain polar angle from the direction of motion receives a Doppler shift in frequency and energy. The actual rest-frame energy for a photon of detected energy E_γ, at a certain angle θ in the laboratory frame, has the following form:

$$E_{\gamma,0} = E_\gamma \frac{1 - \beta \cos\theta}{\sqrt{1 - \beta^2}}$$

Given the β measurements from the separators and the γ-ray emission angle, computed with the help of MINOS vertex tracker and DALI2 geometry, a Doppler correction is applied to the whole γ spectrum. The γ decays of the daughter nuclei are supposed instantaneous in this step. This means that, if an excited state has a certain lifetime, the actual point of emission of the γ-ray does not coincide with the reaction vertex. In this case, the Doppler correction produces a deformation of the peaks in the energy spectrum, creating a wide tail in the left side of the observed peak.

Due to Compton-scattering, a single γ-ray can lose energy in more than one DALI2 crystal during a single event, therefore the photo-peak efficiency from a single scintillator can be lower than expected. The add-back process can reconstruct a higher fraction of the photo-peak by putting together the energies lost in adjacent crystals up to a certain distance from the first interaction point, which is taken in correspondence of the crystal where the most energetic γ-ray is detected [25].

Chapter 3

Data Analysis

3.1 `Geant4` Simulations

In order to study the experimental energy spectra and determine what γ transitions are involved in the reactions, a dedicated simulation `Geant4` code was used to replicate the response of the DALI2 array to incoming radiation. `Geant4` is a simulation toolkit that is useful to reproduce the interaction of particles with matter [26]. With the application of physical models it can be used to simulate collisions or different processes. In this particular case, the software was provided with the real geometrical and material structure of both MINOS and DALI2 in order to fully simulate actual nuclear reactions performed at RIBF.

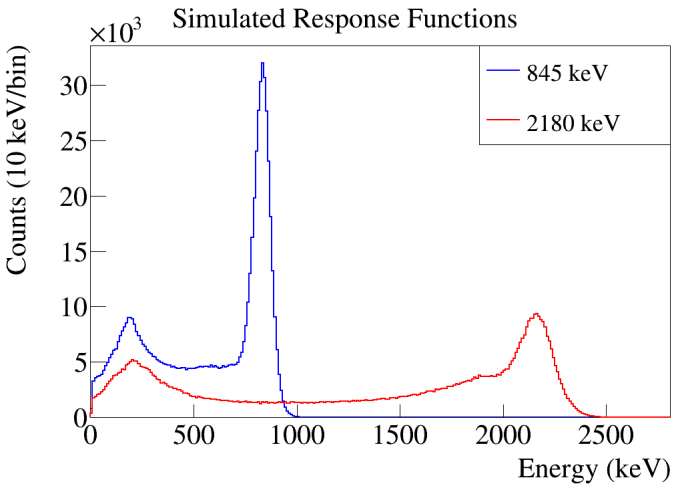

Fig. 4. Simulated response functions on the energy spectrum at 845 keV (simulated with lifetime $\tau = 38$ps [9]) and 2180 keV.

The simulated response functions were employed in the fitting functions for the energy spectra, instead of simpler functions to represent peaks, like gaussians, because of the following reasons. In the first place, the response function gives a reliable profile for the peaks that get detected using the same array, not only to find the photopeak, but also to handle the counts in the Compton continuum correctly, especially in an environment where the low-energy background is so important like this one. Furthermore, the shape of the response of the array varies significantly with the energy of the γ (see Fig. 4), being more asymmetric as the transitions grow in energy, therefore a simple gaussian fit would not represent the shape correctly.

The resolution of NaI scintillators is also not the best to locate single peaks within small energy differences, so the fitting function shape should be as realistic as possible. This simulation has been proven to agree with experimental results and the efficiency agreement is within 6% [27].

The simulation follows three different steps, taking the necessary parameters from input files.
The `EventGenerator` simulates the interaction between the projectile nucleus and the target. The possible excited states of the daughter nucleus are modifiable as parameters and they are the most important settings in order to study a particular γ decay. It is also possible to set the lifetime of the single excited states. Energy losses in the target are taken into account for both the species before and after the reaction.
Each γ transition was simulated individually, as if it existed an excited state of that energy that decayed directly to the ground state. The lifetimes of these simulated excited states were almost all supposed to be equal to zero, given no literature that reports a longer lifetime. The only non-zero lifetimes taken into account in the simulation were those of the $(2^+ \rightarrow 0^+)$ and the $(4^+ \rightarrow 2^+)$ transitions, whose measures are reported in [9]. The lifetime of the 6^+ state was supposed equal to 0 in the fitting process, although its value was measured in [15], but the consequences of the lifetime of this state are discussed in the analysis.

The next step is called `EventBuilder` and its job is to simulate the detection of the γ-rays by the

DALI2 array. The precise geometry and resolution of the crystals are included to have realistic results. This step is useful to study the efficiency of the array.

Lastly, simulated events are processed by the `Reconstructor`, a *ROOT* macro that takes care of the Doppler correction and the add-back procedure. In order to reach more precision in the Doppler correction this step is repeated twice: in the first iteration, the first interaction point of the γ-rays inside the crystals is simulated through a probability distribution, while the second time the code uses the generated first interaction point to perform the Doppler correction on the detected energies. This procedure provides an improvement compared to the Doppler correction made using the center of the crystal to calculate the scattering angle.
The add-back procedure consists in recovering full-energy peaks for single photons, by putting together the low-energy interactions in neighbouring crystals due to the Compton scattering. The maximum distance from the first interaction point taken into account in this process is specified in the input files, and in this case this parameter was set at 15 cm, which is the same distance used for the analysis of the experimental data.

3.2 Fitting procedure

The next step of the work is fitting the energy spectra from the reactions. The procedure that I followed was to simulate 1000000 events of emitting a γ-ray at a certain energy with the `Geant4` software and then take the exact histogram from the simulation output (with Doppler correction and add-back already applied) and use it as part of the fitting function in the experimental spectrum. With the help of *ROOT*, the profile of one single simulated histogram was turned into a user-defined function with two parameters: one for the energy shift, necessary since the exact energies of the detected transitions are unknown in the first place, and one for the amplitude to match the different number of counts in the experimental spectrum. The shift parameter was initially given a broad range ($\pm$50 keV) in order to determine the value for the convergence of the fit. Once the proper value was found, the range was narrowed up to $\pm$10 keV to have a more precise value of the parameter from the fit.
Several of these functions (I will refer to them as *peaks*) were added to the total fitting function, one for each transition to be determined. It is useful to notice that the simulation takes into account all the geometric properties and efficiency of the array, so the amplitude parameter of the fitted peaks is reliable, and if it gets multiplied by the number of simulated events (10^6) it gives an estimation of the actual emitted γ-rays relatively to the simulated transition.
Along with the peaks, a background function was included in the fit: this was made of two exponential functions $e^{C+\lambda \cdot E}$, one for low energies and one for high energies, each one with a slope λ and a constant C, that were employed to model the background noise in the spectra. The reason for choosing exponential functions for the background in the low-energy region of the spectrum is that having a highly-energetic beam and flying fragments induces many atomic excitations in the detectors, as well as in the target, that cause X-ray emissions. Their distribution has been proven consistent with an exponential function [25]. At higher energies in the spectrum, the background is not caused by atomic emissions, but by random nuclear excitations in the apparatus, and also this phenomenon is well approximated by an exponential [25].

In order to quantify how much the presence of a peak is important in the fit, I have applied a *significance* selection. This was done by plotting (see Fig. 5) the amplitude of each peak on the x-axis with the corresponding error on the y-axis and executing a linear fit ($ax + b$) of the points that had the highest amplitudes (the threshold was set accordingly to the dataset). The linear function was to represent the trend of the error at a given number of the counts under the peak. The intercept b of this function gives the error at 0 counts, which is proper to the background, so I defined the significance level of a peak as $S = \dfrac{Amplitude}{b + \sqrt{b}}$, that is the ratio between the number of counts under the peak and the number of counts of the background plus its error and it is measured in units of σ [28].

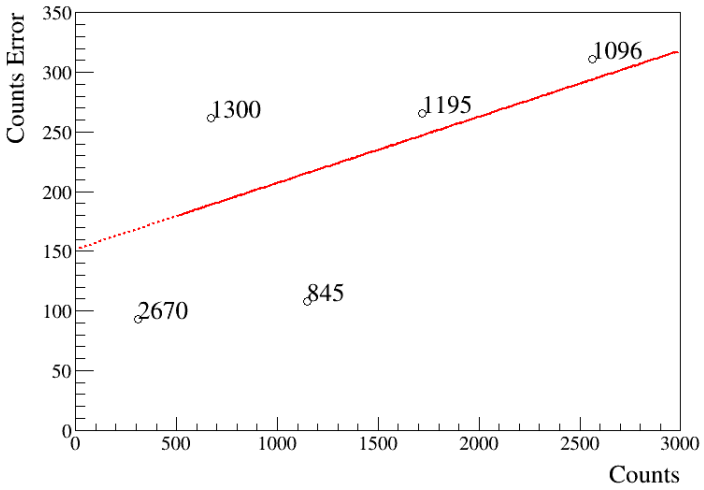

Fig. 5. Linear fit for estimating the background counts and compute significance S. This picture comes from the fit on the $(p, 2p)$ reaction spectrum (see Table 2).

3.3 Fitted spectra and results

3.3.1 Reactions spectra

The first part of the process was to fit the γ spectra for the two reactions with the simulated response of the DALI2 array. For the (p, pn) reaction I chose to fit the spectrum with multiplicity ≤ 3, meaning that the spectrum selected only the events which were found to have at most three γ-rays in coincidence after the add-back. For the $(p, 2p)$ reaction, due to the significantly lower statistics, I chose multiplicity ≤ 4.
The fit was performed on the range $[150, 4500]$ keV, since at higher energies the counts are so low and the relative fluctuations are so large, that it can be assumed to be all background; at lower energies, instead, the histograms peak at around 100 keV due to a threshold set in the detector to cut lower energies, therefore the lower limit of the fitting range is taken after the profile of the histograms is sufficiently regular. I began from the known transition energies of 1096(2) keV ($2_1^+ \rightarrow 0_1^+$) and 845(2) keV ($4_1^+ \rightarrow 2_1^+$) [8], which I simulated with the reported state lifetimes of $\tau(2_1^+) = 7(1)$ ps and $\tau(4_1^+) = 38(9)$ ps [9]. These were in both reactions among the most intense lines.

For the rest of the spectrum, I simulated γ-rays with no lifetime in the excited states, setting the energy in correspondence with a visible increase in counts with respect to the fitted background. For the lines with lowest amplitudes, the presence is not absolutely certain. They were added to have a better fit and I chose to keep them in the final fit only if their significance S was above the unity. Anyway, most of the peaks fitted in the whole spectrum were confirmed later in the coincidence analysis. The existence of some of these smaller peaks, in some cases, could also serve as a compensation of a possible lifetime effect of the excited states. In fact, if a state had a long lifetime, the Doppler correction would produce a wide tail to the left of the peak, and without knowing it, fitting another peak in the left side could adjust the fitting function.
Fig. 6 and 7 show the final fits obtained respectively for the neutron knockout and the proton knockout. As can be seen, for the (p, pn) reaction a total of 13 peaks were necessary to fit the spectrum. In addition to the $2^+ \rightarrow 0^+$ and $4^+ \rightarrow 2^+$ transitions, peaks are visible between 600 and 700 keV, as well as below 500 keV, where there is a distinguishable region where the number of counts is above the exponential background. Due to the width of the peak corresponding to the 2^+ transition, two more lines were fitted to the right (at 1200(13) and 1323(18) keV) and one to the left (at 1004(14) keV). As can be seen in the log-scale plot, an increase in counts above 2 MeV allowed for the inclusion of two high-energy transitions, at 2182(25) and 2359(25) keV. The peaks with values of significance above 10 σ can be regarded as completely established, although the limited resolution and the dense

distribution of peaks in this total spectrum might not give the best estimation of the actual energy of each one. The most significant peaks correspond to the following energies: 363(5), 431(5), 695(7), 829(8), 883(12), 1004(14), 1090(11) and 1200(13) keV.

For the case of the $(p, 2p)$ reaction, only 5 lines were needed in the fit. The explanation might be that fewer states were populated by the reaction, but the significantly lower statistics, compared to the neutron knockout, was a limit in being more precise in the fitting. The four most significant lines are at 859(10), 1081(13), 1171(19) and 1291(29) keV. They can be identified with lines that appear also in the (p, pn) reaction, although the energy values are not exactly the same. For example, the 4^+ line in the $(p, 2p)$ reaction seems to be shifted around 30 keV higher in energy compared to the (p, pn) reaction, whereas the two peaks on the right of the 2^+ give lower slightly lower energy values than in the (p, pn) reaction. A high-energy line at 2710(27) keV could be fitted in this spectrum and this does not seem to have a corresponding transition in the other reaction. Although, the actual presence of this line is in doubt, because it has a significance of $1.9\,\sigma$, which is barely above the acceptance limit.

In Tables 1 and 2, I report the results for the fit on the (p, pn) and $(p, 2p)$ reaction, respectively. Each table shows the final energy E_f, which consists in the simulated energy plus the shift given after the fitting procedure, the amplitude multiplied by 10^6 and reported as N number of counts under the peak, the ratio N/N_{2^+} between the counts of a single peak and the counts under the peak that is identified with the decay from the 2^+ state, and the significance S. On the bottom of the tables the χ^2 of the fit is reported, along with the number of degrees of freedom in the fit (NDF) and the probability associated with the obtained χ^2 ($P(\chi^2)$).

E_f[keV]	$N[\cdot 10^3]$	N/N_{2^+}[%]	$S[\sigma]$
297(7)	3.4(7)	4.9(10)	4.9
363(5)	7.27(7)	10.3(11)	10.3
431(5)	9.1(5)	13.1(8)	13.0
615(8)	6.4(8)	9.2(11)	9.2
695(7)	15.5(8)	22.2(14)	22.2
829(8)	37.6(13)	54(3)	53.9
883(12)	10.4(10)	15.0(17)	14.9
1004(14)	12.4(15)	18(3)	17.7
1090(11)	69.7(19)	100(-)	99.8
1200(13)	19.2(8)	27.5(13)	27.5
1323(18)	4.9(9)	7.0(12)	7.0
2182(25)	3.9(5)	5.6(7)	5.6
2359(25)	2.8(6)	4.0(9)	4.0
χ^2	NDF	$P(\chi^2)$	
192.9	115	0.000007	

Table 1. Fit parameters for neutron knockout - multiplicity ≤ 3. The table shows the final energy of the peak E_f, the number of counts under the peak N, the ratio between the peak amplitude and the 2^+ line amplitude N/N_{2^+} and the significance S.

E_f[keV]	$N[\cdot 10^3]$	N/N_{2^+}[%]	$S[\sigma]$
859(10)	1.15(11)	45(7)	7.0
1081(13)	2.6(3)	100(-)	15.6
1171(19)	1.7(3)	67(16)	10.5
1291(29)	0.7(3)	26(12)	4.1
2710(27)	0.31(9)	12(4)	1.9
χ^2	NDF	$P(\chi^2)$	
102.4	95	0.284	

Table 2. Fit parameters for proton knockout - multiplicity ≤ 4. The table shows the final energy of the peak E_f, the number of counts under the peak N, the ratio between the peak amplitude and the 2^+ line amplitude N/N_{2^+} and the significance S.

For the uncertainty of the E_f, the error given by the fit on the shift was added in quadrature to a systematic error of 1% of E_f. The nature of this systematic error comes from the precision of the detectors, which scales with the energy of the detected γ, and also from the unknown lifetimes of the states, that might affect the centering of the peak in the fit; the error on N was taken directly from the fit and the error on the ratio N/N_{2^+} was given by propagation of the errors of the two parameters, considering also the covariance between the two terms in the fit.

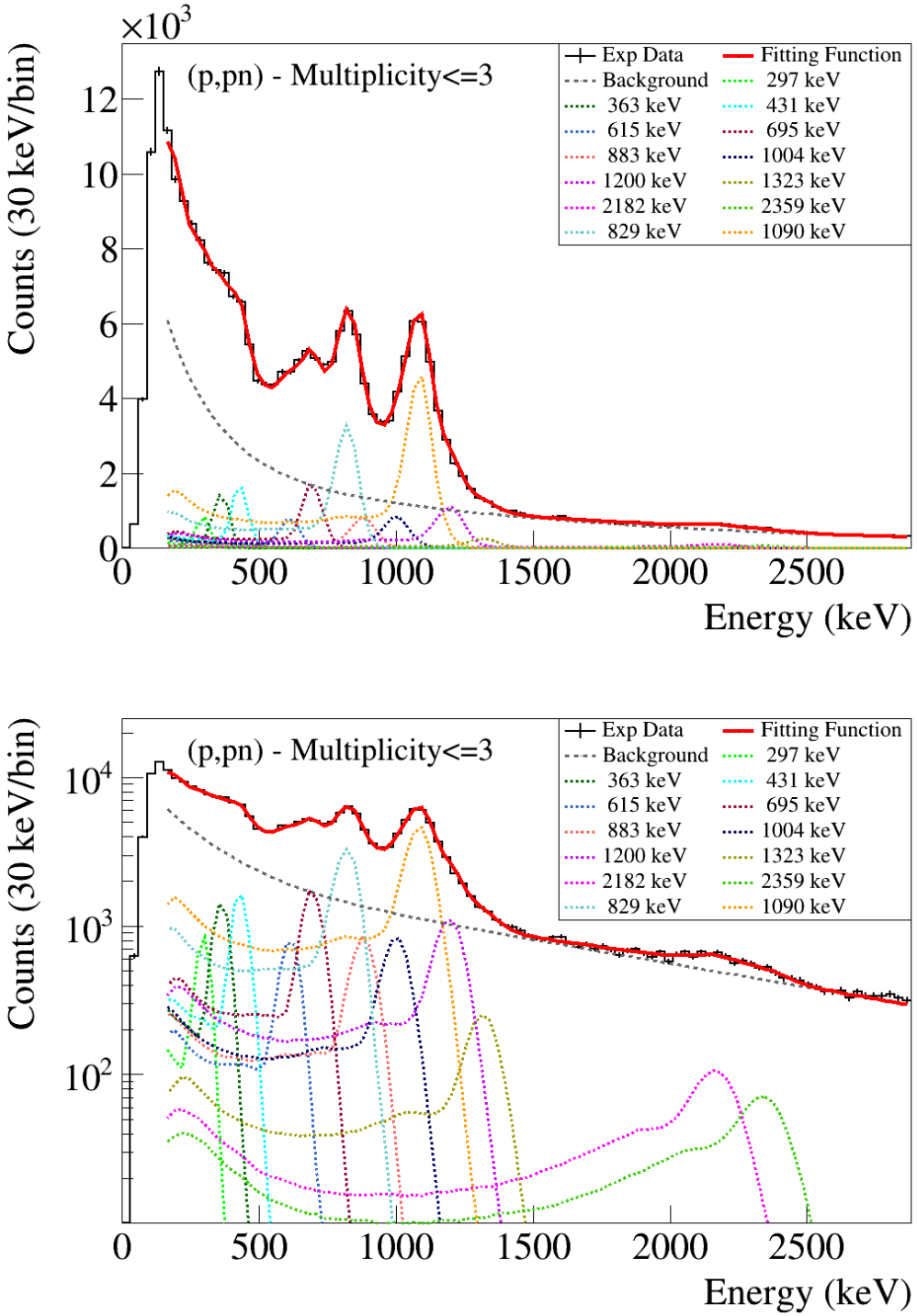

Fig. 6. Fit on the spectrum of the neutron-knockout reaction. Linear scale is represented on the top, log-scale on the bottom. The coloured dashed lines represent the simulated responses of the DALI2 array, the solid red line is the fitting function and the background is displayed with a grey long-dashed line.

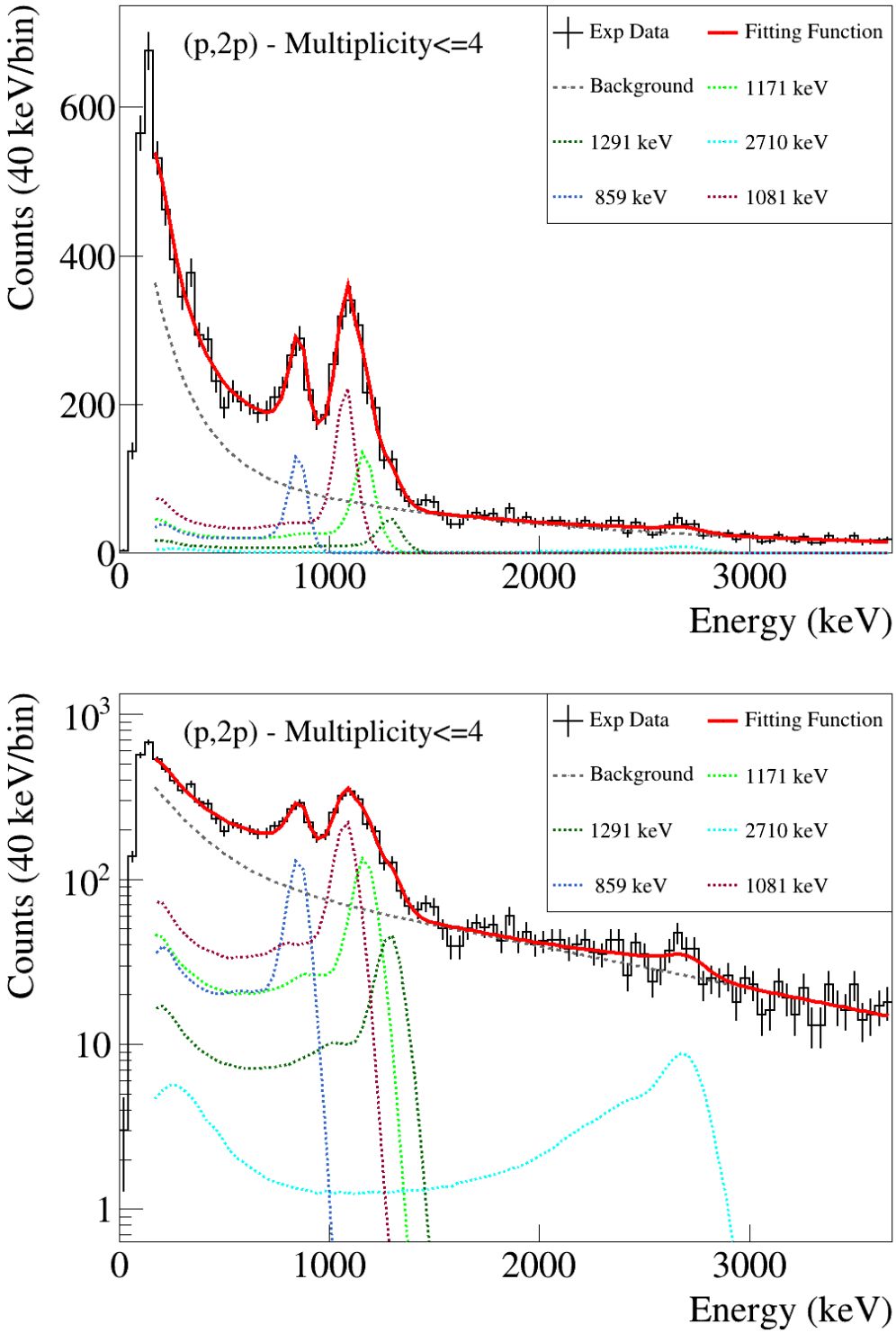

Fig. 7. Fit on the spectrum of the proton-knockout reaction. Linear scale is represented on the top, log-scale on the bottom. The coloured dashed lines represent the simulated response of the DALI2 array, the solid red line is the fitting function and the background is displayed with a grey long-dashed line.

3.3.2 Coincidences spectra

In order to construct a level scheme of the excited states, it is essential to understand which transitions happen in the same event as others. For example, if the 4^+ state at 1941(3) keV [8] is populated by the reaction, both the γ-rays at 845(2) keV ($4^+ \rightarrow 2^+$) and at 1096(2) keV ($2^+ \rightarrow 0^+$) are expected to be detected by the array in the same event. Therefore, by taking the $\gamma - \gamma$ coincidence matrix and projecting on the y-axis a selected number of bins of the x-axis, corresponding to an energy range, a spectrum is constructed with γ-rays only in coincidence with other γ-rays in that energy range.

The most intense line in the (p, pn) spectrum was the one fitted at 1090(11) keV, which can be identified with the 2^+ first excited state [8]. By gating in the center of this peak we get the spectrum in Fig. 8 with the peaks listed in Table 3. For this gate a background subtraction was executed. The operation was performed by taking the histogram gated in [1600,1800] keV, a region where no peak is evident, and subtracting to the 2^+ gated histogram the counts bin-by-bin, renormalized to the gate width. This procedure helps to avoid part of the random coincidences, yet it cannot isolate perfectly the events in coincidence only with the wanted peak. To obtain a better background subtraction, a background gate immediately before and after the peak would be needed, but in this case, due to the limited energy resolution and the very close proximity of several peaks, it is not possible to employ such a technique. This leads to the presence of random coincidences which affect the fitting of peaks in the gated spectra and in particular they can be visualized noticing the self-coincidence of the peaks in their own gated spectra.
As shown in the pictures, the most intense peak in the 2^+ gate is the one at 827(10) keV which corresponds to the γ decaying from the first 4^+ state to the 2^+. The effect of the imperfect background subtraction can be seen here, as the same 2^+ peak has a very high intensity in coincidence with itself, although due to DALI2 limited resolution, it cannot be excluded that another line is present at the same energy. Other peaks which have a significant number of counts are the ones at 432(7) keV, at 684(9) keV, at 883(27) keV and at 1180(14) keV and they all correspond to lines fitted also in the full spectrum, with similar energy values to the ones found there. Furthermore, as can be seen in the log-scale plot, both high-energy transitions that appeared in the whole spectrum can be seen, although their intensities are rather low.

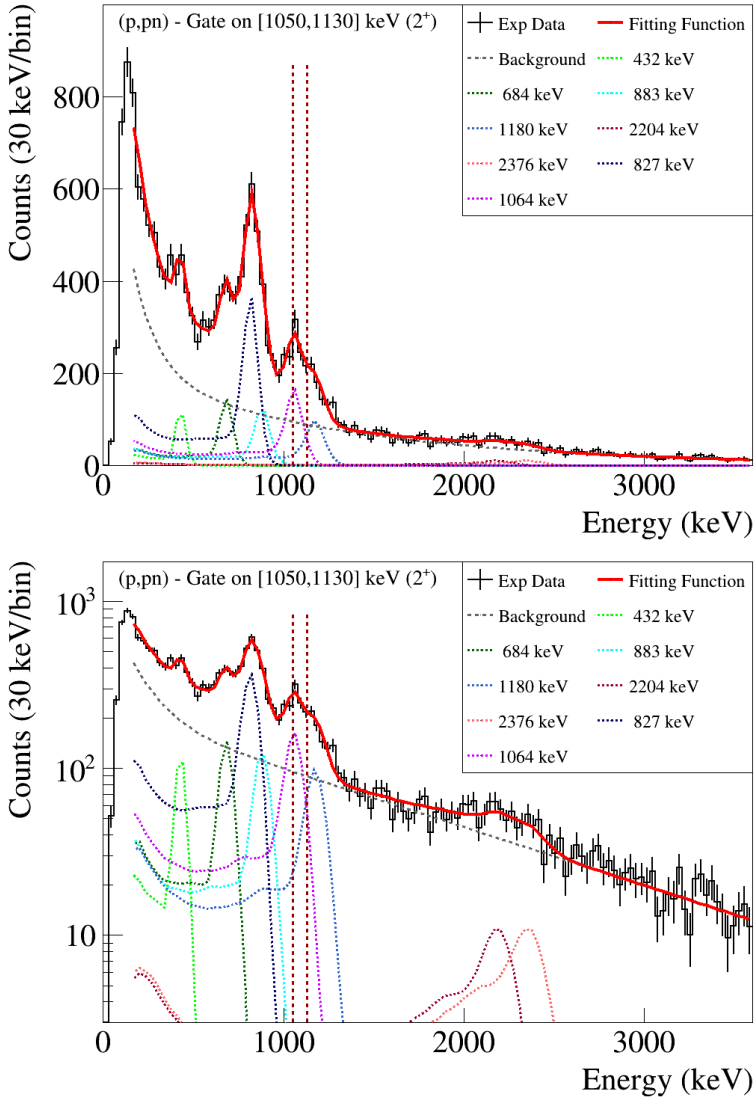

Fig. 8. Fit on the spectrum of the neutron-knockout reaction, gated on [1050,1130] keV (2^+). Linear scale is represented on the top, log-scale on the bottom. The coloured dashed lines represent the simulated response of the DALI2 array, the solid red line is the fitting function and the background is displayed with a grey long-dashed line. The vertical brown dashed lines highlight the range of the gate.

E_f[keV]	$N[\cdot 10^3]$	N/N_{2^+}[%]	$S[\sigma]$
432(7)	0.64(13)	0.91(18)	2.5
684(9)	1.25(15)	1.8(2)	4.9
827(10)	4.3(5)	6.1(7)	16.8
883(27)	1.5(5)	2.2(7)	5.9
1064(12)	2.5(2)	3.5(3)	9.7
1180(14)	1.6(2)	2.4(3)	6.5
2204(45)	0.4(2)	0.6(3)	1.6
2376(54)	0.4(2)	0.6(3)	1.7
χ^2	NDF	$P(\chi^2)$	
138.9	125	0.187	

Table 3. Neutron knockout - Gate on $[1050, 1130]$ keV (2^+). The table shows the final energy of the peak E_f, the number of counts under the peak N, the ratio between the peak amplitude and the 2^+ line amplitude in the (p, pn) full spectrum fit N/N_{2^+} and the significance S.

Then I proceeded with a gate in the identified $4^+ \rightarrow 2^+$ transition, at around 840 keV. Results are shown in Table 4 and Fig. 9. The background subtraction performed in this spectrum was the same as the previous fit, with the background gate in the range [1600,1800] keV, as it was in most of the gated spectra for the (p, pn) reaction. In this gate, as expected, the 2^+ line can be seen very intensely, as it is predictable that every time the 4^+ state is populated, the characteristic γ of the 2^+ is emitted as well. On the left side of the 2^+ peak, another peak at 1008(15) keV is fitted, whose intensity is particularly strong in this spectrum. Due to its proximity to the 2^+ peak, it is reasonable to argue that it might not be an actual peak, but just the aforementioned lifetime effect for the 2^+ state. This might mean that either the 2^+ state or the states above it that feed it could have a lifetime that is longer than the simulated one. Given that the 2^+ lifetime was already measured, the most likely hypothesis is that the effect is due to lifetimes of the feeders.
The lines at 430(7) keV and 690(8) keV have a significance of $3\,\sigma$ and $5.8\,\sigma$ respectively, therefore they must be in coincidence with the 845-keV line. Because of their presence also in the 2^+ gate, I can place both these transitions on top of the 4^+ state. It can be argued that they represent two different branches because the counts for the two peaks are very different, therefore it is less likely for them to be on top of each other. The peak at 1183(17) keV is still very intense, although it is in part covered by the larger 2^+ signal; nevertheless it is reasonable to affirm that it is in coincidence with the 4^+.
The peak at high energy at 2163(32) keV, although with a low significance, is also visible in the log-scale plot of this spectrum, so it could be a transition on top of the 4^+.
Though their significance is acceptable, the peaks at 357(10) keV and 1323(22) keV could also not be present, because they have few counts. In the next gates their existence will be discussed.

E_f[keV]	$N[\cdot 10^3]$	N/N_{2^+}[%]	$S[\sigma]$
357(10)	0.36(12)	0.51(18)	1.4
430(7)	0.79(13)	1.13(19)	3.0
690(8)	1.53(16)	2.2(2)	5.8
830(10)	1.39(17)	2.0(2)	5.3
1008(15)	1.7(5)	2.5(8)	6.5
1092(13)	5.9(5)	8.5(7)	22.3
1183(17)	1.1(4)	1.6(5)	4.2
1323(22)	0.29(16)	0.4(2)	1.1
2163(32)	0.51(14)	0.7(2)	1.9
χ^2	NDF	$P(\chi^2)$	
154.8	123	0.0275	

Table 4. Neutron knockout - Gate on $[790, 860]$ keV (4^+). The table shows the final energy of the peak E_f, the number of counts under the peak N, the ratio between the peak amplitude and the 2^+ line amplitude in the (p, pn) full spectrum fit N/N_{2^+} and the significance S.

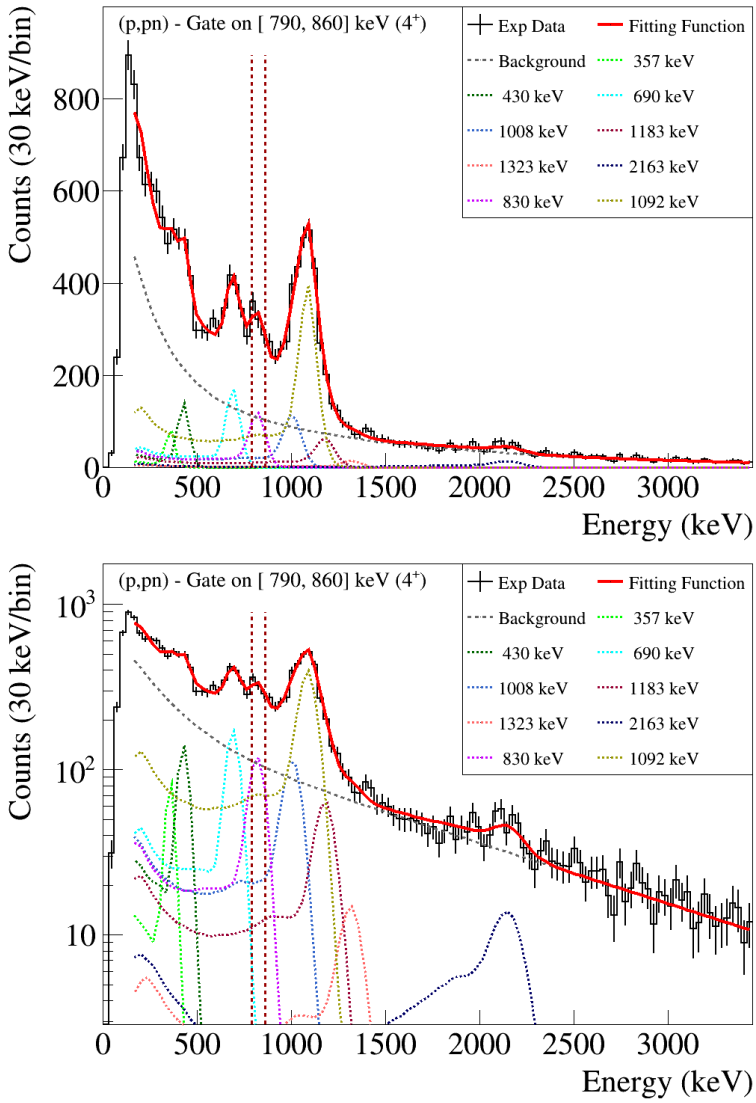

Fig. 9. Fit on the spectrum of the neutron-knockout reaction, gated on [790,860] keV (4^+). Linear scale is represented on the top, log-scale on the bottom. The coloured dashed lines represent the simulated response of the DALI2 array, the solid red line is the fitting function and the background is displayed with a grey long-dashed line. The vertical brown dashed lines highlight the range of the gate.

The next gate in exam is the one on the 690-keV line, the results of which are shown in Table 5 and Fig. 10. Since this transition was placed on top of the 4^+, the intensities of both the 4^+ and the 2^+ lines would be expected to be high and roughly the same value, since every decay to the known 4^+ state would imply also the presence of both those lines.
From the fit it can be seen that the lines at 830(9) and 1071(12) keV are indeed very intense, yet the counts of the 2^+ peak are roughly 50% more than the ones under the 4^+ peak. Apart from these two known transitions and a self-coincidence due to the background, the only two transitions that are significant are the ones at 379(6) keV, which appears in this spectrum clearer than before, and the 1182(19) keV, which has a significant intensity. The line at 301(7) keV has a decent significance, but its actual presence is rather doubtful, because the profile of the histogram does not show a very sharp increase in counts at that value of energy, therefore it could be just out of background fluctuations.

E_f[keV]	$N[\cdot 10^3]$	N/N_{2^+}[%]	$S[\sigma]$
301(7)	0.31(9)	0.44(13)	2.6
379(6)	0.68(10)	0.97(15)	5.6
689(11)	0.66(13)	0.95(19)	5.5
830(9)	2.56(17)	3.7(3)	21.2
1071(12)	3.8(3)	5.4(4)	31.2
1182(19)	0.9(3)	1.3(4)	7.7
χ^2	NDF	$P(\chi^2)$	
174.8	129	0.0045	

Table 5. Neutron knockout - Gate on [660, 720] keV. The table shows the final energy of the peak E_f, the number of counts under the peak N, the ratio between the peak amplitude and the 2^+ line amplitude in the (p, pn) full spectrum fit N/N_{2^+} and the significance S.

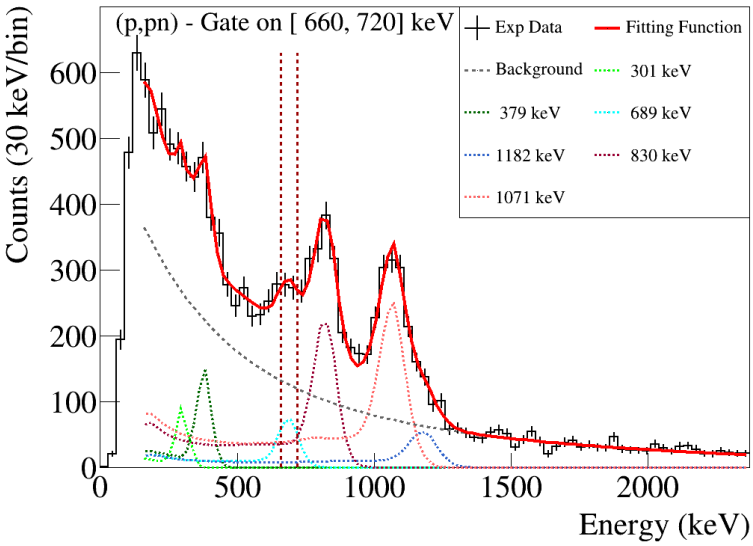

Fig. 10. Fit on the spectrum of the neutron-knockout reaction, gated on [660,720] keV. The coloured dashed lines represent the simulated response of the DALI2 array, the solid red line is the fitting function and the background is displayed with a grey long-dashed line. The vertical brown dashed lines highlight the range of the gate.

For the examination of the gate on the previously seen 1180-keV line, the results are shown in Table 6 and Fig. 11. The gate is not exactly centered on the peak, but it includes only its right side, because in the whole spectrum (see Fig. 6), the 2^+ peak covered with its area about a half of this 1180-keV peak, therefore the decision to gate only on the right part is to avoid including in the gate too many events coming from the 2^+ peak. The most intense lines we see in coincidences are the 2^+ and 4^+, confirming that the 1180-keV is on top of both. Then a self-coincidence is seen, which is probably due to random effects. The peak at 696(36) keV has an acceptable significance, but the amplitude has a large error, therefore it could be present only out of random coincidences.

E_f[keV]	$N[\cdot 10^3]$	N/N_{2^+}[%]	$S[\sigma]$
696(36)	0.26(10)	0.37(15)	1.6
857(11)	0.77(12)	1.11(18)	4.8
1081(14)	1.5(2)	2.1(3)	9.1
1179(39)	0.4(2)	0.5(3)	2.2
χ^2	NDF	$P(\chi^2)$	
134.1	133	0.458	

Table 6. Neutron knockout - Gate on $[1190, 1280]$ keV. The table shows the final energy of the peak E_f, the number of counts under the peak N, the ratio between the peak amplitude and the 2^+ line amplitude in the (p, pn) full spectrum fit N/N_{2^+} and the significance S.

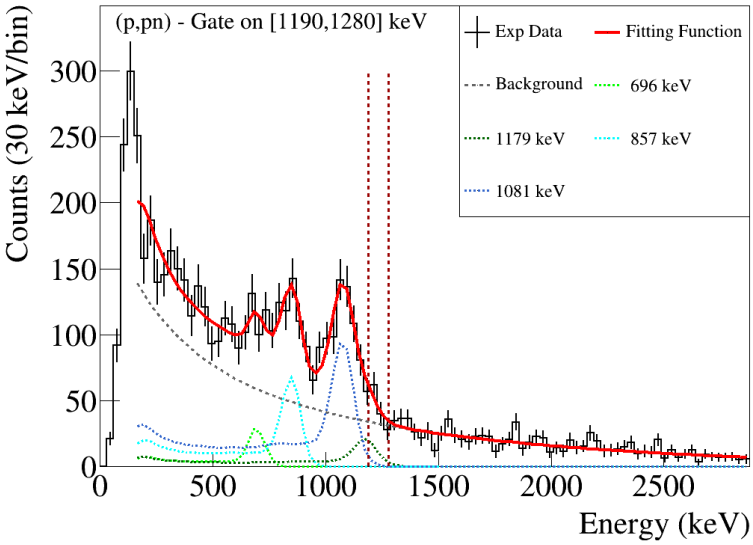

Fig. 11. Fit on the spectrum of the neutron-knockout reaction, gated on [1190,1280] keV. The coloured dashed lines represent the simulated response of the DALI2 array, the solid red line is the fitting function and the background is displayed with a grey long-dashed line. The vertical brown dashed lines highlight the range of the gate.

The gate on the region [400,460] keV (Table 7 and Fig. 12) shows six peaks. Since the gate was performed in region full of atomic background and where all the Compton continua of the higher energy peaks pollute the selection of the events, the gate for the background subtraction was placed in the range [490,570] keV. The 2^+ and 4^+ lines are the most intense and they have roughly the same number of counts, therefore we can confirm the hypothesis of coincidence with both and the placement of the 430-keV line above the 4^+ state.

In the region on the left of the 4^+ peak, 2 peaks that were not found in any of the coincidence spectra can be seen. At 636(15) keV there is a peak that could represent the same transition fitted in the full (p, pn) spectrum at 615(7) keV. The peak at 740(28) keV has never been fitted before but it shows a significance of $2.3\,\sigma$, therefore it could represent a transition that in other spectra was covered in part by the $4^+ \to 2^+$ transition peak. Another peak at 992(32) keV could be identified with the peak seen in the full spectrum and in the 4^+ gate at around 1000 keV. In the low-energy region the relative uncertainties are too large to admit there is more than just background.

E_f[keV]	$N[\cdot 10^3]$	N/N_{2^+}[%]	$S[\sigma]$
636(15)	0.50(16)	0.7(2)	2.3
740(28)	0.5(3)	0.7(4)	2.3
829(15)	1.4(3)	2.0(5)	6.4
992(32)	0.5(3)	0.8(5)	2.5
1078(38)	1.6(4)	2.3(6)	7.5
1195(12)	0.4(2)	0.6(3)	1.8
χ^2	NDF	$P(\chi^2)$	
143.0	129	0.188	

Table 7. Neutron knockout - Gate on $[420, 440]$ keV. The table shows the final energy of the peak E_f, the number of counts under the peak N, the ratio between the peak amplitude and the 2^+ line amplitude in the (p, pn) full spectrum fit N/N_{2^+} and the significance S.

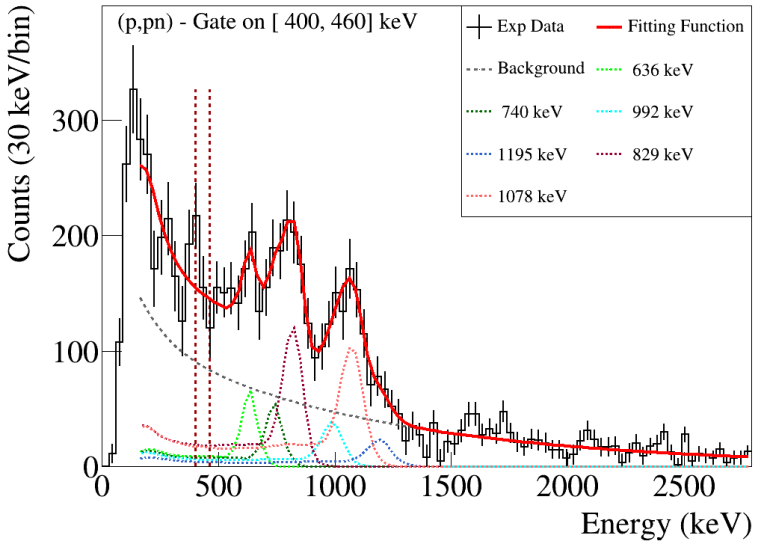

Fig. 12. Fit on the spectrum of the neutron-knockout reaction, gated on [420,440] keV. The coloured dashed lines represent the simulated response of the DALI2 array, the solid red line is the fitting function and the background is displayed with a grey long-dashed line. The vertical brown dashed lines highlight the range of the gate.

Next, the peaks at high energy were checked, and due to their relatively low height in the whole spectrum, I chose to include them both in a wide gate in the range [2000,2550] keV. In this case, the background subtraction was performed by choosing the background gate range at [2600,3000] keV. The resulting spectrum is displayed in Fig. 13 and the fit gives the parameters in Table 8. There are clearly identifiable the 2^+ peak, the 4^+ peak and the 1161(25) keV peak, which can be identified with the peak at roughly 1190 keV in the other spectra, that appears a bit shifted to the left. A peak at 412(11) keV also shows a decent significance. This could be identified with the same 430-keV peak seen before, but the shift is quite large.

E_f[keV]	$N[\cdot 10^3]$	N/N_{2^+}[%]	$S[\sigma]$
412(11)	0.42(12)	0.60(18)	8.5
838(16)	0.57(17)	0.8(2)	11.5
1073(26)	1.5(4)	2.1(5)	30.0
1161(25)	1.0(3)	1.5(5)	20.8
χ^2	NDF	$P(\chi^2)$	
112.50	97	0.134	

Table 8. Neutron knockout - Gate on $[2000, 2550]$ keV. The table shows the final energy of the peak E_f, the number of counts under the peak N, the ratio between the peak amplitude and the 2^+ line amplitude in the (p, pn) full spectrum fit N/N_{2^+} and the significance S.

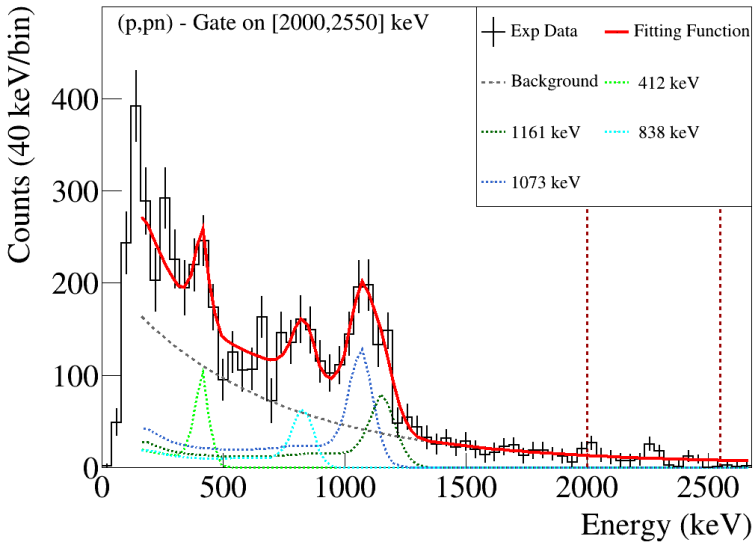

Fig. 13. Fit on the spectrum of the neutron-knockout reaction, gated on [2000,2550] keV. The coloured dashed lines represent the simulated response of the DALI2 array, the solid red line is the fitting function and the background is displayed with a grey long-dashed line. The vertical brown dashed lines highlight the range of the gate.

Then I continued to analyse the gates on the proton-knockout reaction. In the whole spectrum the visible peaks are definitely fewer than the other reaction channel and the statistics is in overall lower. Therefore I performed gates only on the two most intense lines, which are the 2^+ and the 4^+.

As for the gate in the 2^+ (Fig. 14), only three peaks appear in coincidence. First of all, the 4^+, which is a bit shifted to the right compared to the fits performed in the other reaction channel. This behaviour can be observed directly in the whole $(p, 2p)$ spectrum, too, but it cannot be said if there is another peak beneath it, because the errors are rather large. I assume in this case that the 4^+ peak in this reaction and the one fitted in the neutron knockout are the same peak, but the shift could arise from a difference in the reactions. The fitted peak at 1108(21) keV should correspond to the 2^+, but it is a bit shifted to the right, as well. The peak at 1229(39) keV cannot be associated directly to one of the peaks fitted in the full spectrum, because it would have a large shift compared both to the 1171(19) and the 1291(29) keV, and its error on the amplitude is very high.

E_f[keV]	$N[\cdot 10^3]$	N/N_{2^+}[%]	$S[\sigma]$
868(14)	0.21(4)	8(2)	3.2
1108(21)	0.29(8)	11(4)	4.3
1229(39)	0.17(8)	7(3)	2.5
χ^2	NDF	$P(\chi^2)$	
73.6	80	0.68	

Table 9. Proton knockout - Gate on $[1030, 1140]$ keV (2^+). The table shows the final energy of the peak E_f, the number of counts under the peak N, the ratio between the peak amplitude and the 2^+ line amplitude in the $(p, 2p)$ full spectrum fit N/N_{2^+} and the significance S.

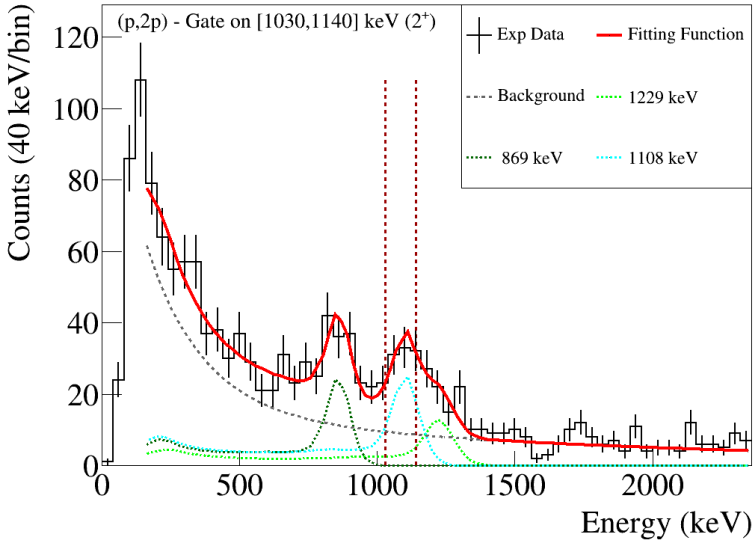

Fig. 14. Fit on the spectrum of the proton-knockout reaction, gated on [1030,1140] keV (2^+). The coloured dashed lines represent the simulated response of the DALI2 array, the solid red line is the fitting function and the background is displayed with a grey long-dashed line. The vertical brown dashed lines highlight the range of the gate.

At last the gate at the energy corresponding to the $4^+ \rightarrow 2^+$ transition of the $(p, 2p)$ spectrum was examined. The coincidence with the 2^+ is confirmed also in this reaction channel, since it is the most intense peak. The self-coincidence is present, probably due to random coincidences. Then the line at 1219(24) keV is present as it is in the 2^+ gate, although this line does not correspond closely to any line fitted in the full spectra of any of the two reactions.

E_f[keV]	$N[\cdot 10^3]$	N/N_{2^+}[%]	$S[\sigma]$
850(17)	0.12(3)	4.5(14)	4.2
1083(17)	0.21(4)	8(2)	7.9
1219(24)	0.14(4)	5.6(17)	5.3
χ^2	NDF	$P(\chi^2)$	
73.56	80	0.681	

Table 10. Proton knockout - Gate on [820, 890] keV (4^+). The table shows the final energy of the peak E_f, the number of counts under the peak N, the ratio between the peak amplitude and the 2^+ line amplitude in the $(p, 2p)$ full spectrum fit N/N_{2^+} and the significance S.

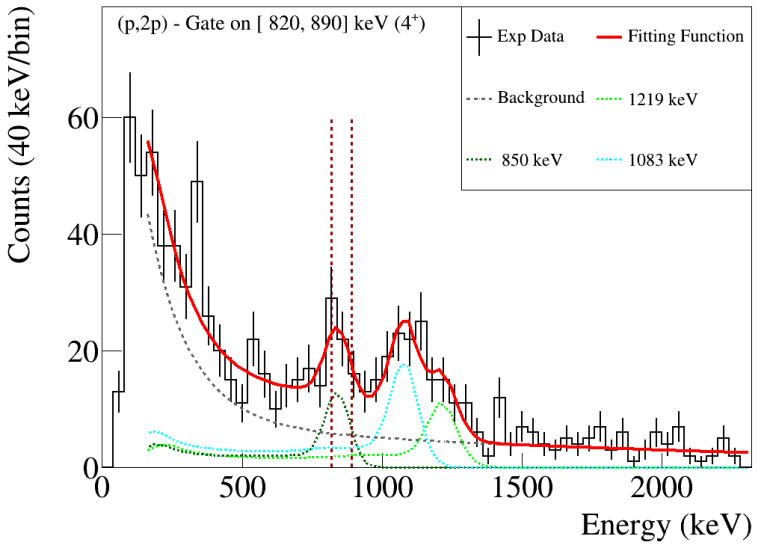

Fig. 15. Fit on the spectrum of the proton-knockout reaction, gated on [820,890] keV (4^+). The coloured dashed lines represent the simulated response of the DALI2 array, the solid red line is the fitting function and the background is displayed with a grey long-dashed line. The vertical brown dashed lines highlight the range of the gate.

3.4 Experimental Level Scheme

From the obtained coincidence spectra it is possible to start drawing conclusions on the ordering of the γ transitions.

The most intense line in the whole spectrum for both reactions (see Tables 1 and 2 and Fig. 3 and 4) are the lines at 1090(11) keV for the (p, pn) and at 1081(13) keV for the $(p, 2p)$, which correspond to the reported 2_1^+ [8]. The second most intense line in the (p, pn) is at 829(8) keV and the third most intense line in the $(p, 2p)$ is at 859(10) keV. These are assumed to represent the same $4_1^+ \rightarrow 2_1^+$ transition [8]. Proof of the cascade of these two lines is that in the 2_1^+ gate for the (p, pn), the 827(10)-keV line is by far the most intense and vice versa: in the 4_1^+ gate for the (p, pn), the 1092(13)-keV line has the highest counts. In the same gated spectra for the $(p, 2p)$, the behaviour is not as evident as the other reaction, but it is still noticeable, despite the lower statistics.

Another intense line in the (p, pn) spectrum is the one at 695(7) keV. This peak appears very significantly also in the 2^+ gated (at 684(9) keV) and in the 4^+ gated spectra (at 690(8) keV), and it is particularly evident in the latter, therefore we can conclude that transition might be on top of the 4^+ state. Further evidence of this cascade is that in the gate in the range [660,720] keV (Table 7), both the $4^+ \rightarrow 2^+$ and $2^+ \rightarrow 0^+$ lines are very intense.

Moreover, in the (p, pn) channel, the 431(5)-keV line belongs to a low-energy bump that cannot be resolved very well in the whole spectrum, but this line appears more clearly in the 2^+ and 4^+ gate, meaning that it is in coincidence with both. Looking at the gates on the previously located 695(7)-keV line (Table 7), the coincidence is not present, therefore the 431(5)-keV transition can be placed directly on top of the 4^+.

The line at 1200(13) keV in the (p, pn) spectrum and the line at 1171(19) keV in the $(p, 2p)$ spectrum

are initially assumed to correspond to the same transition. This seems to have a strong coincidence with the 2^+ in the (p, pn) channel. It has a coincidence also in the 4^+ gate, both in the (p, pn) and in the $(p, 2p)$. In the 430-keV gate, the line is present with a decent intensity. Therefore, it is possible that this transition comes directly on top of the 431(5)-keV line. There are other strange behaviours, though. For example, the line appears with a high significance also in the 690-keV gate, although, according to the hypothesis of coincidence with the 430-keV, the line should not be present. It is also unclear why the 1200(13)-keV intensity in the whole spectrum is much higher that the one of the 431(5)-keV, even if it should be on top and therefore its intensity should be at most the same. This shows that this peak most likely corresponds to more than one transition, making its placement in the level scheme not possible.
The two high-energy peaks, observed in the (p, pn) spectrum at 2182(25) and 2359(25) keV, can be both fitted also in the 2^+ gate, while only a 2163(32)-keV transition is visible in the 4^+ gate. The hypothesis I can make is that the transition represented by the 2182(25)-keV line is directly on top of the 4^+ state , while the position of the 2359(25)-keV transition might be on top of the 2^+ state.
The other high-energy peak that appears only in the $(p, 2p)$ channel at 2710(27) keV does not appear in any gated spectra, therefore it could be a decay directly to the ground state, although the existence of this transition is in doubt due to its low significance.
The lowest-energy peaks are difficult to discuss, because in the whole (p, pn) spectrum, below 500 keV there is a continuum which has definitely more counts than the exponential background, but the exact energies of the peaks are hard to determine. In the $(p, 2p)$ whole spectrum, instead, there might be low-energy peaks, but the relative errors of the bins are too large to assume that there is more than just background. In the 4^+ gate of the $(p, 2p)$ reaction, there is a sharp increase in counts at around 340 keV, but since its width is only one bin I decided to not fit any peak there.
A little higher in energy, a line at 363(5) keV is fitted in the (p, pn) whole spectrum. This line appears in coincidence with both the $4^+ \rightarrow 2^+$ and the 690-keV line and it is especially significant in the latter case. The fact that it does not appear in coincidence with the 2^+ might come from the fact that the maximum multiplicity 3, chosen for the neutron knockout, decreases the probability for a cascade of 4 γ-rays to be detected with all coincidences. Therefore, I can argue that the transition in exam might be on top of the 690-keV.
A peak at 883(12) keV can be fitted in the (p, pn) whole spectrum, as well as in the 2^+ gate. As no other gated spectrum shows this peak, it is reasonable to assume a decay directly to the 2^+. Such a peak is not seen in the whole $(p, 2p)$ spectrum but the explanation could be that due to its proximity to the $4^+ \rightarrow 2^+$ transition, it is difficult to discriminate between these two in a fit, so part of the line could cover counts in the 880-keV peak. This argument is supported by the energy shift of the 4^+ line in Table 2, which is +14 keV, while in the neutron knockout fits, the 4^+ peak tends to have a negative shift compared to the simulated shape.
A peak at 615(8) keV is fitted in the (p, pn) full spectrum with a good significance and the only coincidence in which it appears again is the one in range [400,460] keV, where the peak is at energy 636(15) keV.
The 1323(18)-keV line appears with a modest intensity in the whole spectra of both reactions, but the coincidences are difficult to place, because it only appears in the gate of the 4^+ with a barely acceptable significance.
The peak at 1004(14) keV does not give enough information from the coincidences to make hypotheses on its placement, although from its position really close to the intense 2^+ line in the (p, pn) whole and 4^+ gated spectrum, it could be explained with a lifetime effect on the 2^+ peak. In fact, if the states that feed the 2^+ had a longer lifetime, a tail on the left of the peak would be the result on the spectrum, due to inaccurate Doppler correction for a non-instantaneous decay.
The peaks at around 290 keV (in the full (p, pn) spectrum and the 690-keV gate) and 740 keV (in the (p, pn) 430-keV gate), appear in very few spectra and with a relatively small intensity, so they have been left out of the experimental level scheme. Also the transitions at 883(12) keV, 1004(14) keV, 1323(18) keV (values from the (p, pn) whole spectrum) have not been assigned to a position in the level scheme, because the observed coincidences are not sufficient to characterize their placement, although their presence is significant in several fits.

In Table 11. the final energy values of all fitted peaks are reported, along with the corresponding amplitudes in the reactions spectra. These have been computed through a weighted mean of all the values E_f in Tables 1-10, recognised to belong to the same peak. The formulas for the weighted mean and its statistical error are reported below. The systematic error of the energy is added in quadrature afterwards for these estimations and the large uncertainties for the transitions at 431(26), 832(45) and 1085(72) keV are explained below in this section.

$$\bar{E_\gamma} = \frac{\sum_{i=1}^{n} P_i E_{f,i}}{\sum_{i=1}^{n} P_i} \qquad P_i = \frac{1}{\sigma^2_{E_{f,i}}} \qquad \sigma^2_{\bar{E_\gamma}} = \frac{1}{(n-1)} \left[\frac{\sum_{i=1}^{n} P_i E^2_{f,i}}{\sum_{i=1}^{n} P_i} - \left(\bar{E_\gamma}\right)^2 \right]$$

	(p,pn)		$(p,2p)$	
$\bar{E_\gamma}$	N/N_{tot} [%]	N/N_{2^+} [%]	N/N_{tot} [%]	N/N_{2^+} [%]
299(3)	1.3(3)	4.9(10)	-	-
369(7)	2.7(3)	10.3(11)	-	-
431(26)	3.5(2)	13.1(8)	-	-
618(9)	2.4(3)	9.2(11)	-	-
693(7)	5.9(3)	22.2(14)	-	-
832(45)	14.3(5)	54(3)	11.2(11)	45(7)
883(9)	4.0(4)	15.0(17)	-	-
1005(10)	4.7(6)	18(3)	-	-
1085(72)	26.5(7)	100(-)	25(3)	100(-)
1195(12)	7.3(3)	27.5(13)	17(3)	67(16)
1319(15)	1.9(3)	7.0(12)	7(3)	26(12)
2180(23)	1.5(2)	5.6(7)	-	-
2359(24)	1.1(2)	4.0(9)	-	-
2710(27)	-	-	3.0(9)	12(4)

Table 11. Weighted average values for peak energies and normalized amplitudes for both reaction channels. N/N_{2^+} is the number of counts of the peak normalized to the 2^+ peak in the corresponding whole spectrum; N/N_{tot} is the number of counts of the peak normalized to the integral of the histogram in the fitting range. The large uncertainties of the 431(26), 832(45), 1085(72) keV are discussed later in this section.

In order to discuss the lines in doubt, a comparison will be performed between the obtained coincidences and the experimental level scheme appearing in Ref. [7], result of reactions of β-decay (Fig. 17). From the comparison there can be a better understanding of the coincidences that have been seen. In Fig. 17 I have circled in blue the lines which have been clearly identified with the same placement I assigned, therefore there is a reasonable degree of certainty on the lines at 1085(72), 832(45), 693(7), 369(7), 431(26) keV. The transition at 1195(12) keV is in clear coincidence with the 2^+, 4^+ and 431-keV lines, but it is present also in the 693-keV gate. Furthermore its high intensity in the total, 2^+ gated and 4^+ gated spectra suggests that the hypothesis of it being on top of the 431-keV transition is partially wrong. The likely scenario is that the single peak that has been fitted represents multiple transitions around the same energy and, depending on the gates, one of them is dominant. The transitions in the scheme from the referenced paper that may correspond to this fitted peak at 1195(12) keV are highlighted in yellow. Because of the limited resolution, it is not possible to distinguish different peaks in a region with many counts. Therefore, no transition was placed in the level scheme associated with this energy.

The values for the $2^+_1 \rightarrow 0^+_1$, $4^+_1 \rightarrow 2^+_1$ and $6^+_1 \rightarrow 4^+_1$ transitions seem to have systematic shifts towards lower energies compared with the reported values [8] and also to the level scheme in Fig. 17. This is likely to be linked to a long lifetime of the first 6^+ states: in fact its measured half-life is $t^{6^+}_{1/2} = 860(60)$ps [15]. Therefore, it is possible that with a high population of the first 6^+ state, the peaks associated with the said transitions might have a deformation to the left. The shift effect is especially noticeable on the 4^+ peak in the coincidences of the neutron knockout. This peak undergoes a negative shift of 10-20 keV in almost every case, while in the proton knockout the shift from the reported energy is smaller and to the right. With the 2^+ peak, the behaviour is similar, although not in every spectra in the same measure. Finally, the transition from the almost isomeric 6^+ state to the 4^+ state is always fitted at energy around 430 keV, while the reported value is 454 keV [8].
Since the negative shifts are present almost only in the spectra associated with the neutron-knockout reaction, while in the proton knockout the systematic effect is not seen and the $6^+ \rightarrow 4^+$ peak is not fitted, it is arguable that the 6^+ state associated with the long lifetime is an exclusively neutron-

related excited state. To take into account the deformation induced by the long lifetime, I decided to increase the error bars for the discussed states. To estimate a reasonable value for the systematic scale error induced by the lifetime, I performed a simulation with the reported lifetimes for all three states, generating all excited nuclei in the 6^+ state and, afterwards, a simulation setting the lifetime of the 6^+ to zero, as it was assumed in the fitting section. The comparison produced the shape of the spectra represented in Fig. 16.

It can be seen that the long lifetime of the 6^+ state produces a completely different shape of the spectrum, spreading the counts of the photopeaks in a wide tail to the left. This means that for the events in which the 6^+ state was populated, a deformation towards lower energies is to be considered in the $2^+ \rightarrow 0^+$ and $4^+ \rightarrow 2^+$ peaks. This is likely linked to the fitting of the extra peak at 1005(10) keV which was in the left part of the large 2^+ peak.
A procedure of enlarging the error bars for the final values of the energies of the discussed three peaks can help take into account the deformation. With reference to Fig. 16, the position of the top of the peaks was estimated in the spectrum with and without the 6^+ lifetime, and the relative shift in percentage was taken as an extra term of scaling systematic error, to be added to the previous 1% assigned for the energy of every peak.

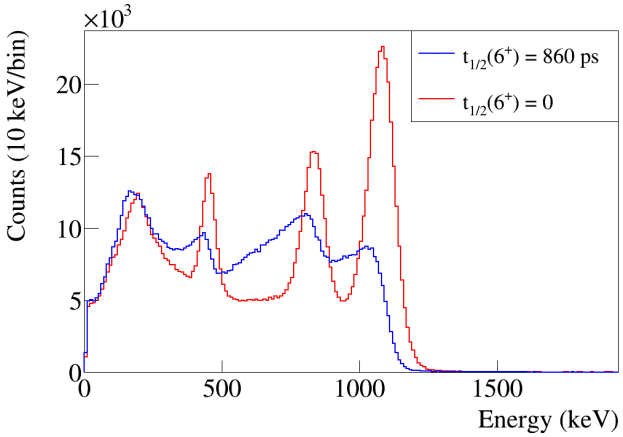

Fig. 16. Simulated response function for the cascade $6^+ \rightarrow 4^+ \rightarrow 2^+ \rightarrow 0^+$ in the case of the lifetime for the 6^+ reported in [15] and in the case of null lifetime.

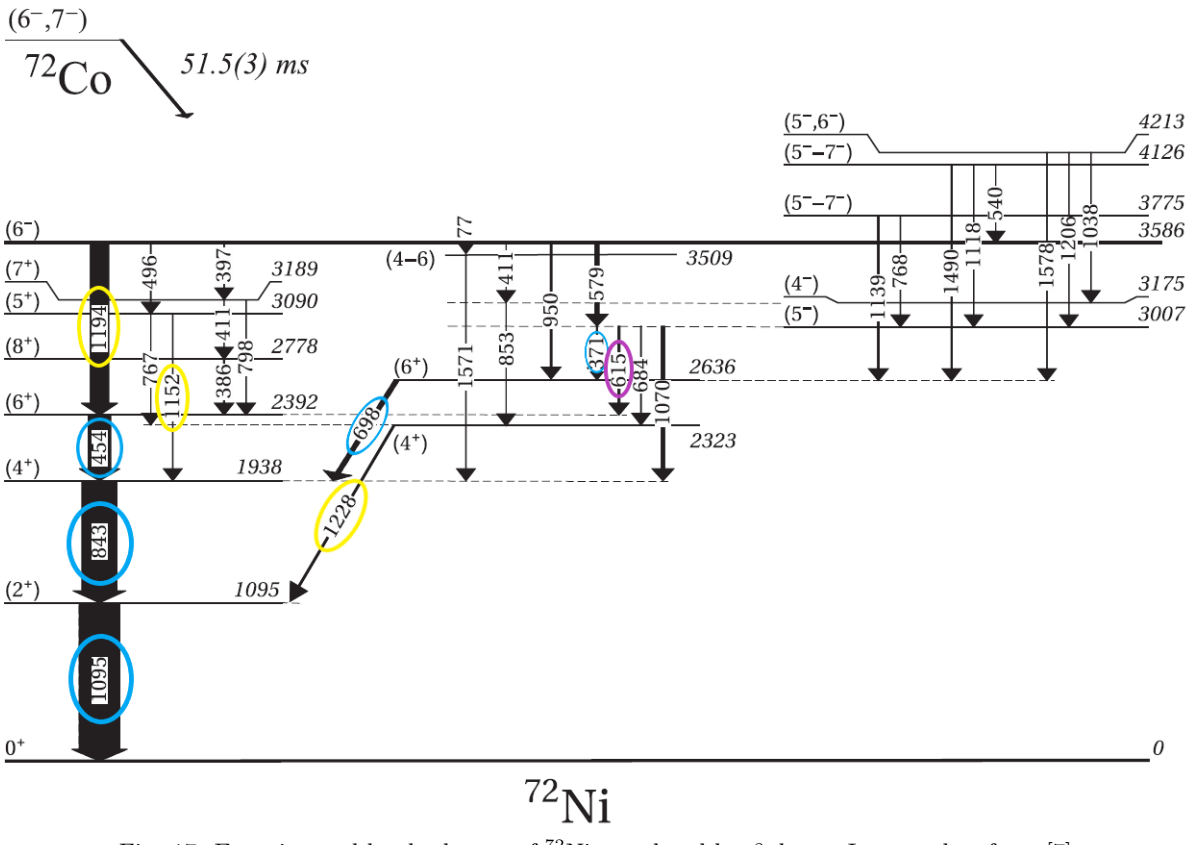

Fig. 17. Experimental level schemes of ^{72}Ni populated by β-decay. Image taken from [7].

The purple-circled line in Fig. 17 refers to the transition I found at 618(9) keV, which appears in the whole (p, pn) spectrum, as well as in the 431-keV gate, therefore it might be in coincidence with this line. The same peak cannot be fitted in the 2^+ or 4^+ gate but it might be because of the higher intensity of nearby transitions. The hypothesis is realistic, since according to Morales *et al.* the 5^- state, from where it decays, is surely populated, in order to allow the transition at 369(7) keV. Moreover, the $5_1^- \rightarrow 4_2^+$ transition at 684 keV that is in Fig. 16 could be present in the (p, pn) spectrum, but it might be indistinguishable from the line at 693(7) keV. That could explain also the presence of a 1182(19)-keV peak in the [660,720] keV gate, since in the scheme the line from 4_2^+ to 2_1^+ is at 1228 keV.

Fig. 18 shows the summary of the transitions which could be positioned in a level scheme from the analysis of the fitted peaks and the coincidences, as well as through the comparison with the Morales level scheme. The energies of the γ-rays are written in blue, while the total energy of the states (with respect to the ground state) are indicated in red. Tentative spins and parities are assigned to the states through the comparison with Fig. 17 and are written on the levels in black.
The γ drawn with a blue continuous line are the ones I am rather sure about; instead, the dashed line represents a transition on which there could be some doubt.

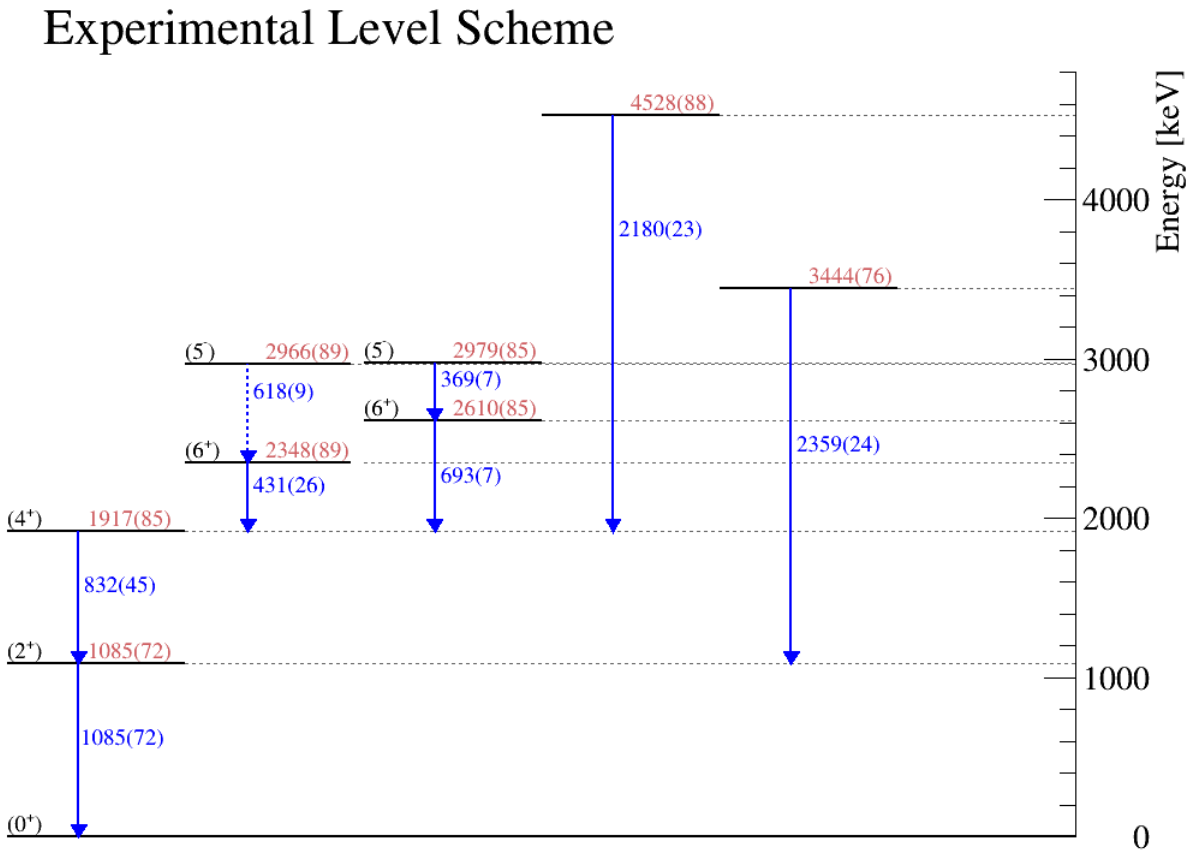

Fig. 18. Experimental level scheme as a result of the coincidence analysis, with tentative spins and parities. State energies in keV are written in red while γ-ray energies are in blue. The transition at 618(9) keV is drawn with a dashed line because its presence is in doubt.

Chapter 4

Results Discussion

4.1 Shell Model Calculations

In order to compare the results obtained from the fitting of the experimental spectra, calculations were made to estimate the energy levels with the relative J^{π} and state populations after the reactions. A quantification of the state populations is given by the spectroscopic factors in the wanted reactions. These are coefficients obtained by integrating the product of the wavefunctions before and after the reaction for each shell model state, so as to have an estimation of the overlap of the initial and final states, which is directly related to the probability of populating a certain final state.
I used the *KSHELL* code [29] to calculate the wanted values. This consists in a user-friendly code to perform shell model calculations, starting from a certain closed-shell nucleus and specifying an interaction between nucleons acting in the wanted valence space. The calculations give values for the energy levels and the associated spins and parities, as well as reduced transition probabilities between levels. If two nuclei are specified, the code computes also spectroscopic factors between the states of the two nuclei.
In this case the nucleon-nucleon interaction *jj4pna* was employed, characterised by the effective interactions matrix elements described in Ref. [30]. The starting core nucleus in the calculations was ^{56}Ni, therefore the valence space was formed by only neutrons, in particular 16 of them for ^{72}Ni.
The ground-state of ^{73}Ni was also calculated, in order to obtain spectroscopic factors for the neutron knockout reaction. The only needed level was the ground state, because the beam is supposed to interact with the target at a time when all possible excited states, obtained in the production of the isotope, would have decayed to the ground state. Unfortunately, the proton knockout could not be characterised by this model. The reason is that the mother nucleus of ^{73}Cu would have a closed 28-proton shell plus only one proton in the valence space. Therefore, since the code can only affect the nucleons in the valence shells, the calculations for a proton-knockout reaction cannot be performed.

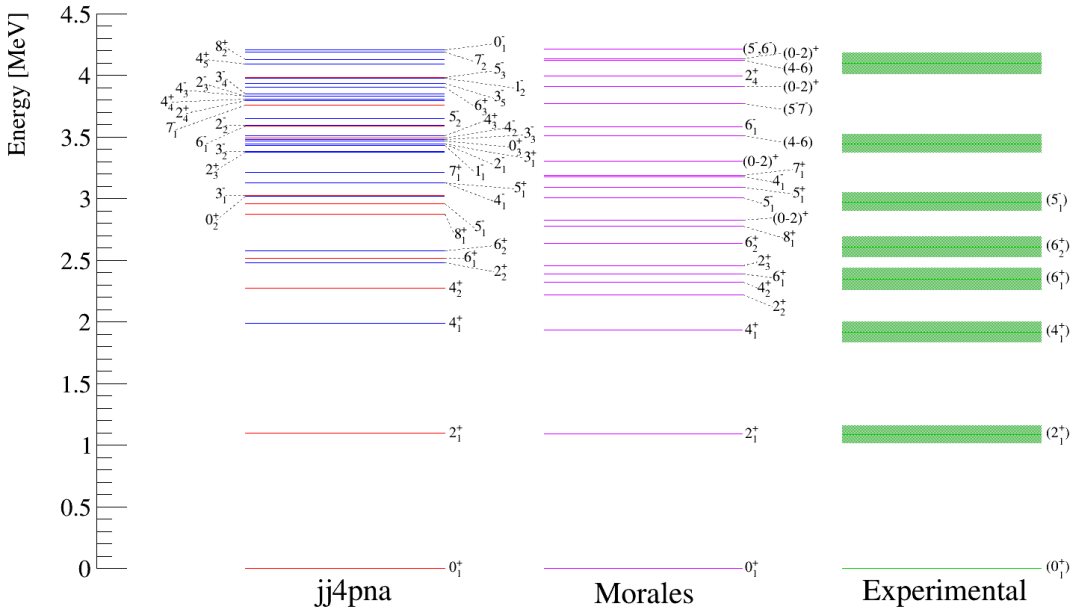

Fig. 19. Comparison of energy levels between the shell model calculations made with the *jj4pna* interaction, the experimental level scheme by Morales from Ref. [7] and the experimental scheme built in this work. The red levels in the *jj4pna* scheme are the ones with a significant spectroscopic factor.

4.2 Comparisons and discussions

In Fig. 19 a comparison of the energy levels is shown. The compared sources are the *KSHELL* shell model calculations with the *jj4pna* interaction, with the lowest 20 states of each parity, the Morales level scheme that appears in Ref. [7], built from a β-decay experiment, and the experimental level scheme of the present work, with the states from Fig. 18. The experimental levels are represented with the error bars as a coloured green area. The only states that have not been assigned any J^π are the ones reached by the high-energy transitions over 2 MeV. These levels are difficult to identify in the other schemes, since they are close in energy to many different levels. The represented value of the (5^-) state energy is given by the weighted average of the two values that are given by the initial energy of the two cascades (369(7)/693(7) keV; 618(9)/431(26) keV) in Fig. 18 and the final value is 2972(75) keV.

Fig. 20 shows the spectroscopic factors given by the calculations with the *jj4pna* interaction for the (p, pn) reaction, highlighting the most probable states in which the daughter-nucleus can find itself in, according to the theory. As the distribution shows, the neutron is most likely removed from the $\nu g_{9/2}$ subshell, which is the one at highest energy. The most probable state given by the theory is the first 8^+ state, which in this analysis was not observed; an inspection of Fig. 17 suggests that it would be associated to a 386 keV transition onto the 6^+_1. Also the 4^+_2 state, which has a high spectroscopic factor, was not observed. By Fig. 17, though, this state could be identified with a transition of 1228 keV onto the 2^+, which could correspond to the transition around that energy that I did not place in the scheme. An alternative explanation could be that, in the calculations, the negligence of the proton interactions could have inverted the energy ordering of the two 4^+ states. The population of the 6^+_1 is in line with the discussion about the effect of deformation of the spectra given by the lifetime of this excited state. States at higher energy show a reasonable spectroscopic factor, but they could not be identified in this analysis. Apart from these, the uncertainty of the identification of the 4^+ and the 8^+ state, the theoretical results look quite consistent with what was found in the experimental data, therefore even without handling the protons, the ^{72}Ni is described reasonably well by this interaction, meaning that $Z = 28$ is confirmed to be a good magic number.

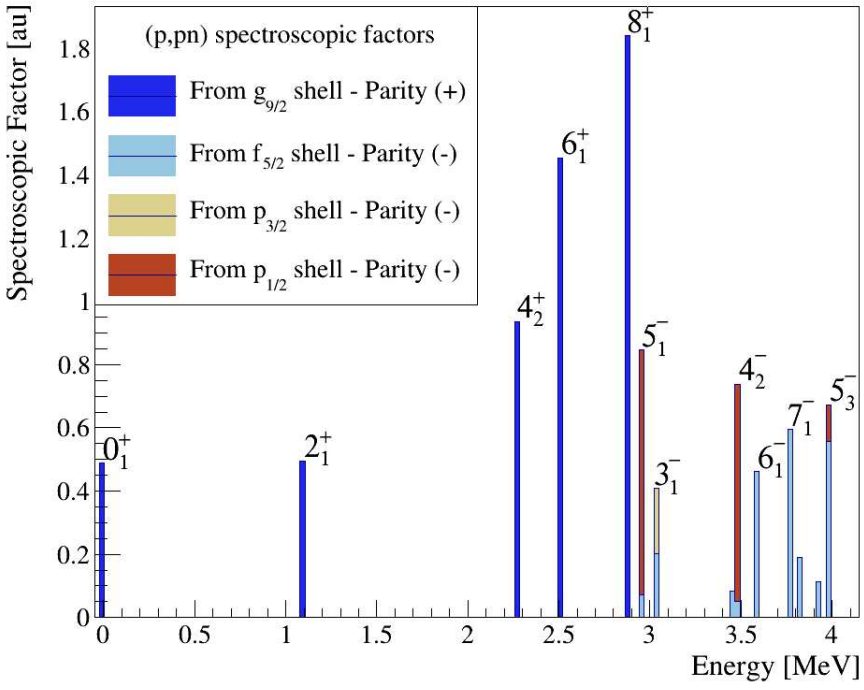

Fig. 20. Comparison of spectroscopic factors from neutron-knockout reaction to different states of ^{72}Ni, divided by the subshell from which the neutron was removed. Calculations were performed with the *jj4pna* interaction

In a similar analysis of ^{70}Ni described in [17], the spectra of the 1-proton and 1-neutron knockout show a similar behaviour to the ones studied in the present work. Of course, the germanium detectors allow for a better resolution of the peaks, but the distribution of the lines for each reaction channel looks similar. For example, in both isotopes the proton-knockout shows a very high intensity only for the 2^+ and 4^+ peaks, although some less intense lines at lower energy can be found in the ^{70}Ni. For the neutron knockout, instead, also in the spectrum of the ^{70}Ni several peaks are found below 700 keV and therefore more states are populated in the reaction, especially a 5^- state that is found through coincidences. In the comparison, the most significant peculiarity in ^{72}Ni is the population of the long-lived 6^+ state, which is symptomatic of the disappearance of the 8^+ seniority isomer present in other nickel isotopes, such as the ^{70}Ni. Therefore, apart from this seniority-related difference, the two neighbouring even-even isotopes show the same behaviour in the spectra associated with the proton and neutron knockout.

Chapter 5
Conclusions and Perspectives

5.1 Conclusions

To sum up the work, two different reactions to populate ^{72}Ni were taken into exam: neutron knockout and proton knockout. The experiment was performed at the RIBF during the first SEASTAR campaign. With the DALI2 response functions simulated with `Geant4`, experimental spectra were fitted and several transitions were observed. Subsequently, from the coincidence analysis, the ordering of the identified transitions was discussed, along with effects given by lifetimes and uncertainties from the limited resolution of the detectors. The (p, pn) reaction spectrum showed several different transitions, while the $(p, 2p)$ reaction seemed to populate fewer states and the significant lines identified in the spectrum were only from the 4_1^+ and 2_1^+ states, although deeper analysis was prevented by the limited statistics. An experimental level scheme of ^{72}Ni was built and the identified energy states are the 2_1^+, 4_1^+, 6_1^+, 6_2^+, 5_1^-, which are reported in previous works, and the two states at 3444(76) and 4528(88) keV were observed, but not identified in previously known levels. Furthermore, the lifetime of the 6_1^+ state was discussed as a feature linked to the disappearance of the seniority isomer in ^{72}Ni, compared to its isotopic chain. The comparison with the shell model calculations, with a valence space populated only by neutrons, shows that the theory agrees partly with the data, although some differences might be induced by the absence of the proton excitations in the model. Finally, the comparison with ^{70}Ni reveals that the two isotopes show similar properties for the spectra associated with the examined reaction channels, except for the presence of a 8^+ seniority isomer in the lighter isotope.

5.2 Future Perspectives

The discussion on the agreement of the theory with the experimental results could be improved if one could perform more complex shell model calculations, that could take into account also the proton excitations and give more unbiased energy levels, as well as spectroscopic factors for the proton-knockout reaction.
The determination of the energy levels could be undoubtedly more precise if the experiment was performed with Ge detectors, since one of the main issues of the analysis in this work is the distinction of different lines in a narrow energy range, that is strongly limited by the resolution of the scintillators in DALI2. Given a better resolution, a more precise analysis of coincidences could also be possible, for the construction of a more complete experimental level scheme.
Seeing the results on both ^{70}Ni and ^{72}Ni, a similar analysis of the same reaction channels could be performed on ^{74}Ni as well, expecting comparable shapes for the spectra to the ones seen here. For that isotope, the disappearance of the seniority isomer is confirmed just as for the ^{72}Ni, therefore a similar lifetime for the 6_1^+ state is predictable, whose effects could be witnessed in the spectra even with data from a detector with limited resolution like DALI2.

Bibliography

[1] L. Fortunato, Appunti di Fisica Nucleare, Gruppo editoriale L'Espresso, 2019

[2] K. Heyde - Basic Ideas and Concepts in Nuclear Physics - IOP Publishing Ltd. - 1999

[3] K. S. Krane, Introductory Nuclear Physics, Wiley, 1988

[4] O. Sorlin, *et al.*, arXiv:0805.2561v1 [nucl-ex], 2008

[5] `http://hyperphysics.phy-astr.gsu.edu/hbase/Nuclear/shell.html`

[6] T. Otsuka *et al.*, Phys. Rev. Lett. 95 (2005) 232502

[7] A. I. Morales *et al.*, Phys. Rev. C 93, 034328 (2016)

[8] National Nuclear Data Center, `http://www.nndc.bnl.gov/`.

[9] K. Kolos *et al.*, Phys. Rev. Lett. 116, 122502 (2016)

[10] R. Taniuchi *et al.*, Nature 569, 53 (2019).

[11] O. Perru *et al.*, Phys. Rev. Lett. 96, 232501 (2006).

[12] T. Marchi *et al.*, Phys. Rev. Lett. 113, 182501 (2014).

[13] P. Van Isacker 2011 J. Phys.: Conf. Ser. 322 012003

[14] C. Mazzocchi *et al.*, Phys. Lett. B 622 (2005) 45-54

[15] A. I. Morales *et al.*, Phys. Lett. B 781 (2018) 706-712

[16] F. Angelini *et al.*, INFN-LNL Report 259 (2020)

[17] B. Elman *et al.*, Phys. Rev. C 100, 034317 (2019)

[18] P. Doornenbal and A. Obertelli., RIKEN proposal for scientific program: Shell evolution and search for two-plus states at the RIBF (SEASTAR), Unpublished, 2013

[19] T. Kubo *et al.*, Prog. Theor. Exp. Phys., 2012(1), 2012

[20] T. Baumann, Minicourse on Experimental techniques at the NSCL - Fragment Separators, 2001

[21] A. Obertelli *et al.*, Eur. Phys. J. A, 50(1), 2014.

[22] Y. Giomataris *et al.*, Nucl. Instr. Methods in Phys. Res. Sect. A, 376(1):29–35, 1996.

[23] SUNFLOWER Collaboration, `https://www.nishina.riken.jp/collaboration/SUNFLOWER/`.

[24] S. Takeuchi *et al.*, Nucl. Instr. Methods in Phys. Res. Sect. A, 763:596–603, 2014.

[25] M. L. Cortés, PhD Thesis, TU Darmstadt, 2016

[26] S. Agostinelli *et al.*, Nucl. Instr. Methods in Phys. Res. Sect. A, 506(3):250-303, 2003.

[27] V. Vaquero, PhD Thesis, UA Madrid, 2018

[28] M. Lettmann, PhD Thesis, TU Darmstadt, 2018

[29] N. Shimizu *et al.*, Comp. Phys. Comm. 244, 372 (2019)

[30] A. F. Lisetskiy *et al.*, Phys. Rev. C 70, 044314 (2004)